AD-A119 730 AIR FORCE INST OF TECH WRIGHT-PATTERSON AFB OH F/G 4/2
MOVING BOUNDARY ISOTHERMAL FOG CHAMBER (MOBIFOC),(U)
MAY 82 G F FISHER
UNCLASSIFIED AFIT/CI/NR/82-52T NL

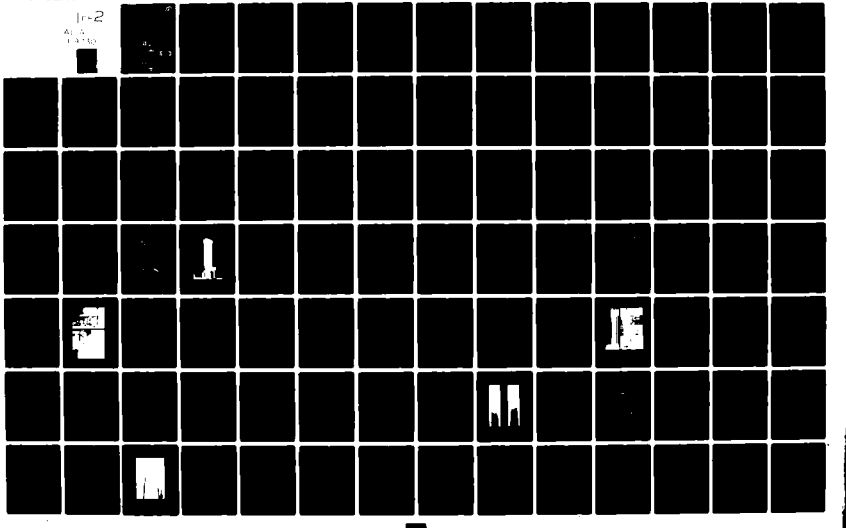

MOVING BOUNDARY ISOTHERMAL FOG CHAMBER (MOBIFOC)

by
George F. Fisher

A Thesis Submitted to the Graduate Faculty of
North Carolina State University
May 1982

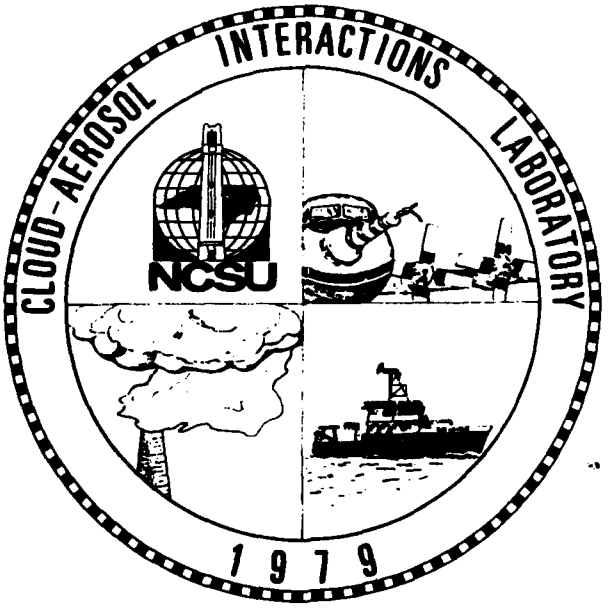

DEPARTMENT OF MARINE, EARTH, AND ATMOSPHERIC SCIENCES
NORTH CAROLINA STATE UNIVERSITY
P.O. BOX 5062
RALEIGH, NORTH CAROLINA 27650

UNCLASS

SECURITY CLASSIFICATION OF THIS PAGE *(When Data Entered)*

REPORT DOCUMENTATION PAGE		READ INSTRUCTIONS BEFORE COMPLETING FORM
1. REPORT NUMBER AFIT/CI/NR/82-52T	2. GOVT ACCESSION NO. AD-A119 730	3. RECIPIENT'S CATALOG NUMBER
4. TITLE *(and Subtitle)* Moving Boundary Isothermal Fog Chamber		5. TYPE OF REPORT & PERIOD COVERED THESIS/~~DISSERTATION~~
		6. PERFORMING ORG. REPORT NUMBER
7. AUTHOR(s) George F. Fisher		8. CONTRACT OR GRANT NUMBER(s)
9. PERFORMING ORGANIZATION NAME AND ADDRESS AFIT STUDENT AT: North Carolina State University		10. PROGRAM ELEMENT, PROJECT, TASK AREA & WORK UNIT NUMBERS
11. CONTROLLING OFFICE NAME AND ADDRESS AFIT/NR WPAFB OH 45433		12. REPORT DATE May 1982
		13. NUMBER OF PAGES 105
14. MONITORING AGENCY NAME & ADDRESS*(if different from Controlling Office)*		15. SECURITY CLASS. *(of this report)* UNCLASS
		15a. DECLASSIFICATION/DOWNGRADING SCHEDULE

16. DISTRIBUTION STATEMENT *(of this Report)*

APPROVED FOR PUBLIC RELEASE; DISTRIBUTION UNLIMITED

17. DISTRIBUTION STATEMENT *(of the abstract entered in Block 20, if different from Report)*

18. SUPPLEMENTARY NOTES

APPROVED FOR PUBLIC RELEASE: IAW AFR 190-17

Lynn Wolaver

LYNN E. WOLAVER
Dean for Research and
Professional Development
AFIT, Wright-Patterson AFB OH

16 SEPT 1982

19. KEY WORDS *(Continue on reverse side if necessary and identify by block number)*

20. ABSTRACT *(Continue on reverse side if necessary and identify by block number)*

ATTACHED

82 09 20 184

DD FORM 1 JAN 73 1473 EDITION OF 1 NOV 65 IS OBSOLETE

UNCLASS

SECURITY CLASSIFICATION OF THIS PAGE *(When Data Entered)*

ABSTRACT

FISHER, GEORGE FREDERICK. Moving Boundary Isothermal Fog Chamber. (Under the direction of VINOD K. SAXENA.)

A new instrument for the study of fog and haze is introduced. The moving Boundary Isothermal Fog Chamber is the first successful attempt to improve upon the operating ranges and reliability of these instruments since they were first introduced 10 years ago. This new concept utilizes moving sidewalls in a rectangular chamber of 2 x 20 x 58 cm and is capable of providing growth times far exceeding those in current instruments. The larger walls of the chamber (20 x 58 cm) are constructed of vulcanized rubber belts covered with a moisture absorbent material (Pellon) which are continually driven by a variable speed motor. The direction of flow is upward against gravity. The result of the marriage of moving sidewalls and upward flow is a nearly plug type flow capable of sustaining large haze droplets for an almost indefinite period of time.

The rate of flow and speed of sidewalls are independently adjustable and for various combinations flow profiles can be varied from pure parabolic with stationary walls to a profile where more than 90% of the chamber has a constant velocity within 5% or less. Isothermal haze chambers currently in use can, at best maintain about 10% of the chamber at constant velocity and since all have the flow in the direction of gravity cannot suspend droplets of any size.

The chamber itself is constructed of aluminum resting in an acrylic framework which supports the chamber and belt mechanism and contains separate water reservoirs for each moving belt which passes

inside the aluminum sidewall. One side of the rectangular chamber can be replaced with clear acrylic for observational purposes. Laboratory tests have been conducted with the observation window in place using both titanium tetra-chloride smoke and laboratory aerosols. Through the use of smoke, the various velocity profiles are easily observed and verified. Residence times for the smoke have easily exceeded 20 minutes and have shown extreme stability of control over individual smoke particles. Tests of laboratory aerosols composed of ammonium sulfate show the same degree of control over haze particles along with the ability to suspend droplets for long periods of time.

Studies are conducted into the approximation formulas used in data reduction. It is shown that growth of sulfate particles from the dry state to haze and fog droplets crucially depends upon their initial dry radii, density and surface tension of solution droplets, concentration of solutes in droplets, and relative humidity of the environment. In this study, it is demonstrated that sulfates are the least water soluble of all the nineteen electrolytes which have been extensively studied. Sulfate droplets between 80% relative humidity and the critical value of supersaturation cannot be regarded to consist of weak solutions - an assumption so commonly used in the study of haze droplets in the isothermal haze chambers. Nineteen common electrolytes have been classified according to their solubility in water and the solution concentrations at whic these may be treated as weak solutions. A method is given to eliminate errors in approximation formulas commonly used in the literature to derive

critical parameters of haze droplets. Two examples of the new method are presented to demonstrate its effectiveness.

The advantages of this unique and innovative instrument are numerous, the least of which is the improvement in growth times over current instruments. The ability to suspend droplets and to directly observe them allow for the study of interaction of various aerosols, chemical processes and studies of visibility in haze. The chamber has also been designed for later application of thermal gradients and therefore for use as a thermal gradient diffusion cloud chamber (TGDCC) which will also have extended growth times over current TGDCC's.

MOVING BOUNDARY ISOTHERMAL FOG CHAMBER

by

GEORGE F. FISHER

A thesis submitted to the Graduate Faculty of
North Carolina State University
in partial fulfillment of the
requirements for the Degree of
Master of Science

DEPARTMENT OF MARINE, EARTH AND ATMOSPHERIC SCIENCE

Raleigh

1982

APPROVED BY:

_____ _____

_____ _____

Chairman of Advisory Committee

MOVING BOUNDARY ISOTHERMAL FOG CHAMBER

by

GEORGE F. FISHER

A thesis submitted to the Graduate Faculty of
North Carolina State University
in partial fulfillment of the
requirements for the Degree of
Master of Science

DEPARTMENT OF MARINE, EARTH AND ATMOSPHERIC SCIENCE

Raleigh

1982

APPROVED BY:

Allen J. Riordan

Vinod K. Saxena
Chairman of Advisory Committee

BIOGRAPHY

George Frederick Fisher was born in Everett, Massachusetts on 20 February 1947. He attended public schools in Massachusetts graduating from Chelmsford High School in 1964. Upon graduation he attended Michigan State University and later transferred to Fitchburg State College, Fitchburg, Massachusetts majoring in mathematics.

In July, 1967, he left school to enlist in the United States Army Finance Corps. After graduating as Honor Graduate from the U. S. Army Finance School, the author was assigned duty in West Germany where he held the position of Deputy Installation Coordinator with the rank of Sergeant until his discharge in July, 1970. He then returned to Massachusetts where he was employed as an accountant for the Alpha Construction Corporation.

In January, 1974, the author enrolled at the University of Massachusetts, Amherst where he also joined the Air Force ROTC program. The author graduated cum laude receiving a Bachelor of Science degree in physics in May 1976 at which time he was also commissioned a second lieutenant in the United States Air Force. He then attended the University of Utah through the civilian institution program of the Air Force Institute of Technology receiving a Bachelor of Science degree in Meteorology in June 1977. He was then assigned duty as Chief Forecaster at the U. S. Army airfield in Hanau, West Germany and later transferred to Ramstein, West Germany where he was a Command Weather Briefer. The author was accepted to the Air Force Institute of Technology and began study toward the

Master of Science degree in Meteorology at North Carolina State University in August, 1980.

He is currently a full member of the American Meteorological Society and is the recipient of numerous military decorations and awards.

The author is married to former Emilie Linke, a native of West Germany.

ACKNOWLEDGEMENT

The author wishes to express his deepest appreciation to those who have made it possible to complete this study. In particular, to his father whose example provided the confidence necessary to proceed in this direction of study and to family and close friends who have provided the necessary moral support.

Special appreciation is extended to the United States Air Force and in particular to the Air Force Institute of Technology and Air Weather Service which have made it financially possible to pursue this study and to the funds provided through grants by the National Science Foundation which have provided the materials and facilities used in the course of study.

He would also like to extend his deepest thanks to Dr. V. K. Saxena, chairman of his advisory committee for providing guidance and encouragement, and most especially for sharing his knowledge with the author. The author also thanks Drs. T. Hauser and A. Riordan for their advice and assistance in preparation and presentation of this study.

He would also like to extend his compliments and appreciation to the machinists in the Physical and Mathematical Sciences department whose superb craftsmanship have contributed greatly to the successful operation of MOBIFOC and to Mickey Wai and Raj Rathore for their computer assistance.

Finally, the author wishes to express his gratitude for the patience of his wife, Emilie, who sacrificed her trip to the beach during the course of this study.

TABLE OF CONTENTS

TABLE OF CONTENTS (CONTINUED)

LIST OF TABLES

LIST OF FIGURES

LIST OF FIGURES (CONTINUED)

CHAPTER 1

1. INTRODUCTION

Aerosols in the atmosphere constitute one of the necessary ingredients in the formation of clouds. The sources and sinks of atmospheric aerosols and the properties, lifetimes and changes undergone by particulate material are of special interest; first, because particles are more readily noticed than the mainly invisible gaseous pollutants, and second because particles are a link in the chain of the removal processes which return gaseous pollutants to the earth's surface. The latter interaction can hardly be overemphasized but it is often overlooked. It is not only the rate of emission of a possible noxious pollutant that matters, but the product of its rate of emission and residence time. The true importance of aerosols has been recognized only in the past twenty years (e.g., Schaefer, 1969) and consequently many of the details of chemical and physical transformations are still obscure.

The necessity of the atmospheric aerosol in producing cloud and precipitation was well established in the late 19th century by such famous investigators as Lord Kelvin, Aitken, and Köhler and is second in importance only to the presence of water vapor in the atmosphere. The interaction of aerosols and water vapor in the atmosphere contribute to climatic change by altering precipitation patterns (Changnon, 1981) influencing storm tracks (Hayashi and Golder, 1981), altering atmospheric heat budget through changes in radiative properties such as turbidity and albedo (McCartney and Unsworth, 1977; Bradley, 1981) and by producing chemical changes in the atmosphere. It is for these

reasons that portion of particulate aerosols referred to as Cloud Condensation Nuclei (CCN) are most important.

With so many aspects of our environment dependent upon the atmospheric aerosols, the need for continued research into this area is imperative. Despite the knowledge we have of the importance of the atmospheric aerosol and the ways that it interacts with and affects our atmosphere, many of the basic questions still remain unanswered such as the origin and "clean" air concentrations of aerosols (Twomey, 1980; Schaefer, 1980; Jayaweera, 1981). The answers to these questions and others lie in the ability of instruments to accurately duplicate and measure the various factors involved in the interaction between aerosols and water vapor (Schaefer, 1971) and to establish a reliable data base for our environment.

1.1 Aerosols and Water Vapor in the Troposphere

The relationship between aerosols and water vapor is of main concern in the troposphere since transport mechanisms, cloud formation and storms are mostly confined to this region of the atmosphere (Byers, 1974). We know that the atmospheric aerosol provides the mechanism for phase transformations of water vapor into liquid water (e.g., Pruppacher and Klett, 1980), and that the diffusion of water vapor is the driving force and dominant mechanism in producing growth (Fuchs, 1959) of cloud droplets. The need to study the atmospheric aerosol is well known to cloud physicists and may be found in any basic text dealing in cloud physics (e.g., Wallace and Hobbs, 1977; Rogers, 1979). For the purposes of this study, the cloud condensation nuclei (CCN) are most important,

and form a central point around which this study centers. As pointed out by Squires (1971) the spectrum of activation, or critical supersaturation of CCN is the preferable method of study since this allows a valid parameterization of the atmospheric aerosol regardless of size, density or chemical composition, quantities which are presently immune to study in the natural environment. This method of parameterization allows us to establish a ratio between water vapor and concentration of aerosols in the atmosphere to gain an understanding of the interaction of those two prime factors. With the help of this data we can further improve our capability to control and modify our weather (Detwiler and Vonnegut, 1981), expand our knowledge of turbidity and albedo dependence on aerosols (Hänel, 1981a; Ryznar et al, 1981) and most importantly, to evaluate the impact of anthropogenic aerosols on weather and climate (Marlow, 1980) - an issue vital to our continued existence on this planet.

1.2 Historical Development of Instrumentation

Instrumentation used in the study of aerosol-water vapor interactions have emerged in discreet steps rather than as a continuous improvement in design. They can therefore be classified into three distinct categories characteristic of their modes of operation and application to the field of study. These categories are: expansion cloud chambers, diffusion cloud chambers and isothermal haze chambers. Further, diffusion cloud chambers may be subdivided into two types: the chemical gradient diffusion cloud chamber and thermal gradient diffusion cloud chamber.

The value of these instruments can never be over-estimated since nearly all knowledge of cloud formation and aerosol-rain cloud interactions has been gained through their use. Furthermore, the full potential of instrumentation of this type has yet to be realized. A larger portion of the value of these instruments lies in the simplicity of the basic principles behind their operational modes and designs. However, this same simplicity places severe limitations which provide the main reason for the three instrument types. Following is a brief discussion of each class of instrument and its applications.

1.2.1. Expansion Cloud Chamber. One of the first expansion cloud chambers in existence appeared around 1670 when von Guericke (1602-1686) used the instrument to examine cloud particles. The first experiments with this chamber dealing with the atmospheric aerosol came 200 years later when Coulier (1824-1890) demonstrated the role of dust particles in causing the phase transition from vapor to liquid droplets. Refinement of the expansion cloud chamber was brought about between 1880 and 1900 by Aitken (1829-1919) and Wilson (1869-1959) whose names are frequently associated with this type of chamber (Pruppacher and Klett, 1980).

The basis of operation of the expansion cloud chamber is the rapid adiabatic expansion of moist air producing unnaturally large supersaturations. Since these supersaturations are of several hundred percent relative humidity (Amelin, 1967), nucleation of pure water vapor into liquid droplets occurs and nearly all atmospheric aerosols activated. The main drawback of this chamber in the study of CCN is the supersaturations are 1-5 orders of magnitude higher than that

naturally found in the atmosphere (Sedunov, 1974; Twomey, 1959) and that the clouds produced are of short duration due to vapor depletion and thermodynamic considerations (Vietti and Schuster, 1973; Berg and George, 1968). An excellent review and discussion of expansion cloud chambers as they are used today can be found in Kassner et al, (1967).

1.2.2. Diffusion Cloud Chambers. Diffusion cloud chambers first appeared when Langsdorf (1936) developed a Chemical Gradient Diffusion Cloud Chamber (CGDCC) for use in nuclear physics. Its use was limited to detection of nuclear particles until Schaefer (1952) refined the instrument for use in cloud physics. The CGDCC took advantage of various geometries to allow water vapor to diffuse from a water source toward a chemical solution whose equilibrium vapor pressure is lower than that of water, thereby producing supersaturations between the two. The advantages of this instrument are that supersaturations typical of those found in the atmosphere during typical cloud formation processes could be duplicated, and since they operated in an isothermal mode, they were convectively stable (Squires, 1972). Some problems did exist with this type of chamber which not only limited its use but also affected the reliability of measurements obtained. The most serious of these deficiencies was again the basic principle of operation which employed the use of chemical solutions. As water vapor diffused into the solution (usually HCl) the solution became diluted, the equilibrium vapor pressure over the solution was increased, and the supersaturation inside the chamber was continually changing. Second the chemical solution also caused contamination of the sample air passing through the chamber.

In order to provide a more reliable instrument, Wieland (1956), Twomey (1962) and Severynse (1964) introduced and made operational the Thermal Gradient Diffusion Cloud Chamber (TGDCC). Using geometries similar to the CGDCC, the TGDCC allowed water vapor to diffuse between two water surfaces which were at different temperatures and therefore had different equilibrium vapor pressures. Since temperatures are easily maintained within $0.1^{o}C$ excellent control of supersaturations is attained and therefore measurements become reliable with no chance of contamination of sample. The TGDCC opened new horizons in the study of CCN and much time has been dedicated to constructing and improving various configurations of these instruments as evidenced by the number of workshops devoted almost entirely to instrumentation (Grant, 1971; Kocmond et al., 1981). The earlier of these instruments had many limitations. The most serious of these was the resolution time involved in gathering the activity spectrum of CCN. Since only one supersaturation can be measured at one time, 30 minutes or longer is required to complete one spectrum. This made them impractical for use in airborne experiments (Braham, Jr., 1974; Changnon et al., 1975) since the time necessary was sometimes longer than the entire lifetime of the cloud. Two instruments standout as overcoming these difficulties (Fukuta and Saxena, 1979b; Radke et al., 1981) and represent the state of the art in TGDCC development.

The instrument of Radke et al cleverly combines four separate TGDCC's into one instrument with each chamber operating at a different supersaturation. This method allows simultaneous study of the supersaturation spectrum between 0.2 and 1.5% supersaturation at 4 discreet

points along the spectrum. Fukuta and Saxena, however, have produced an instrument which not only produces thermal gradients across the chamber, but also along the top and bottom of chamber (Fukuta and Saxena, 1979a) and through a unique method of supplying water vapor provides a continual spectral analysis of the activation of CCN over the entire supersaturation range of 0.15% to 1.2% every 15 seconds. Much literature is available on the principles of operation and limitation of these instruments such as Saxena and Kassner (1970) Saxena and Carstens (1971), DeSalmand and Serpolay (1982) and Alofs and Carsten (1976).

1.2.3 Isothermal Haze Chambers. Although it is true that the TGDCC is by far the most important instrument yet to be used in studying the CCN spectrum, it still has a severe limitation in that it is incapable of examining the spectrum below a supersaturation of 0.15%. This portion of the spectrum is not of much consequence in cumulus type clouds where supersaturations are normally much higher, but is of importance in long lived clouds such as stratus or in the formation of fog and haze (Mason, 1960; Hudson, 1980; Gerber, 1981). This limitation is imposed primarily due to the residence time needed to activate droplets at the lower supersaturations (Saxena and Carstens, 1971; Hudson and Squires, 1976) and therefore a method is needed to provide longer growth times. It has been shown that the TGDCC is incapable of providing these growth times (Sinnarwalla and Alofs, 1973). The Isothermal Haze Chamber (IHC) was first introduced by Laktionov (1972) to provide the necessary longer growth times.

The principle of operation of this chamber involves subjecting aerosols to an environment of 100% relative humidity. Using relationships discussed later in this thesis which are based on growth equations developed by Köhler (1936) and as detailed by Laktionov (1972), the activation spectrum below 0.15% obtained. To date this method is restricted to the range 0.015 to 0.15% (Fitzgerald et al., 1981) due to availability of limited growth times. A summary of operational characteristics and problems of the IHC is given in Chapter 2 of this study.

1.3 Need for Improved Instrumentation

The Isothermal Haze Chamber was first used for CCN spectrum determination in the Soviet Union in 1972 (Laktionov, 1973). Intermittent uses over the next few years were seen (e.g., Fitzgerald, 1978; Hoppel, 1979) but full use of the instrument did not arise until about 3 years ago by investigators such as Hudson (1980) and Alofs and Liu (1981). Theoretical calculations and observations (Gerber, 1981) both show that fogs (visual range < 1 Km) can exist at relative humidities near 99% to supersaturations above 0.1%. Clearly, to gather details of the microstructure of fogs, improvements are needed to the isothermal haze chamber to allow study of the activation spectrum below 0.15% supersaturation. This research is dedicated to that need and represents development of an instrument capable of the task.

1.4 Requirements of an Improved IHC

In order to meet the needs of studying spectra below 0.15%, the need for a longer residence, or growth, time is a prime requirement. This could be easily achieved in most of the existing instruments by simply extending the length of the chamber, but this solution makes the instrument too unwieldy for any practical use. A method of operation is therefore needed which keeps the size and weight of instrument at a minimum, yet allows extended growth times not currently available.

In addition to the prime requirement, other features are desirable which will add to the versatility of the instrument. Some of these are:

a. Operation at less than 100% relative humidity

b. Operation as a TGDCC

c. Direct observation of sample for studies of droplet growth, turbidity, and chemical/physical interactions.

d. Mobility.

This research paper presents a new isothermal haze chamber which because of its application to fog studies is called the Moving Boundary Isothermal Fog Chamber (MOBIFOC) and currently allows for incorporation of the above listed requirements.

1.5 Objective of the Present Study

The objective of this research is to design and fabricate a prototype isothermal haze chamber which will provide prolonged growth times. To this end, moving boundaries (chamber walls) are incorporated which provide a uniform and stable velocity profile

regardless of the flow rate in the chamber. Completion of this initial phase includes final construction and documentation that desired velocity profiles are present and that moisture fields are as expected. Construction designs will take into consideration the desire to apply temperature gradients, portability and direct observation capabilities for later implementation.

This thesis is organized into six chapters including the introduction. Chapter 2 deals with IHC's developed to date with details of their operational characteristics and emphasis on their advantages and disadvantages. Chapter 3 outlines the techniques and procedures followed in the development and fabrication of MOBIFOC while Chapter 4 presents proof of the ability to meet the requirements and goals established for the prototype model. Chapter 5 discusses sources of error in data reduction while Chapter 6 is a conclusion and suggestions for further development and experimental use of MOBIFOC.

2. ISOTHERMAL HAZE CHAMBERS

The isothermal haze chamber (IHC) as used in studies of CCN spectra was first brought to public notice only ten years ago (Laktionov, 1972) in the Soviet Union. During the last decade only a few select groups have devoted time to constructing and improving these instruments. Foremost in this research are Desert Research Institute (DRI) at Reno, Nevada and the University of Missouri, Rolla (UMR) at Rolla, Missouri. All the instruments to date have the same general features in common. These are vertical positioning and sample entry at top with downward flow. These particular features make these chambers extremely simple to produce, maintain and operate. The prime advantage of the IHC as it exists is not however, its simplicity, but the opportunity it affords to study the activation spectrum below 0.15% supersaturation.

2.1 Basis of Development

Saxena and Carstens (1971) computed the growth time required for a droplet to grow from its equilibrium size at 100% relative humidity to its critical size under an applied supersaturation slightly higher than the critical supersaturation. These computations are reproduced in Figure 2.1. The main feature of note on this figure is that at supersaturations below 0.1%, activation times become alarmingly large (Laktionov, 1967; Saxena and Carstens, 1971). As growth times increase, the exposure time (or residence time) inside the chamber must also increase in order to distinguish activated CCN from inactivated haze droplets (Squires, 1971). Additionally, the size of droplets increase as the critical supersaturation decreases (Rogers, 1979) and so,

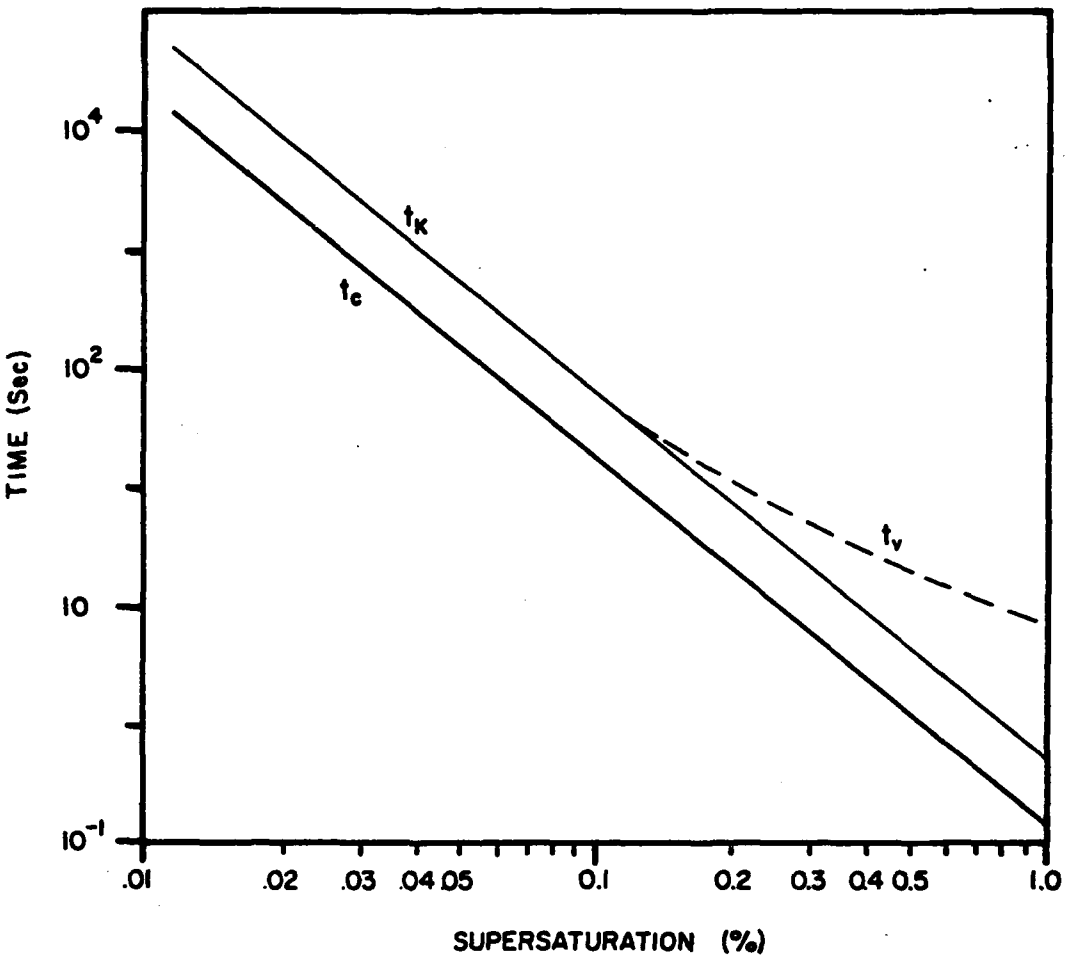

Figure 2.1 Plot of growth time vs. supersaturation for NaCl solution droplets. Time (t_c) required for a solution droplet of NaCl to grow to its critical radius from its equilibrium radius at 100% relative humidity. Also indicated are times required to reach the critical radius of an equivalent pure water droplet (t_k) and to reach a minimum detectable size of 1μ (t_v) under the same conditions. (After Saxena and Carstens, 1971.)

therefore, does the settling velocity. Limitations on the aspect ratio (width to height) of TGDCC's (Twomey, 1963; Squires, 1971) cause droplets to settle out of the chamber prior to activation making this instrument unreliable below 0.15% supersaturation.

Aleksandrov et al. (1969) calculated growth times for water droplets to reach their equilibrium size at 100% relative humidity. Their results showed that growth times under these conditions are considerably less than the times required to reach critical size. Laktionov (1972) realized that this provided a method to study the activation spectrum at low supersaturation and used the results to design the first IHC to be used for this purpose. The fifth chapter in this thesis explores the theoretical basis which Laktionov used in detail, so the discussion presented here will focus only on the design considerations of IHC's to date and not on the methods of data reduction.

2.2 Instruments Currently in Use

The isothermal haze chamber operates on a simple and basic principle. Water vapor is supplied inside a chamber which is held at 100% relative humidity. Aerosols are then passed through the chamber and exposed to this environment for sufficient length of time so that droplets grow to at least 95% of their equilibrium size at 100% relative humidity. To date all chambers have been designed for residence times of 180-200 seconds. This time is based on computations by Aleksandrov et al. (1969) which indicate that this is the time necessary for CCN composed of NaCl which are activated at 0.016% supersaturation to grow to their equilibrium size at 100% relative

humidity from their initial droplet dry size. This therefore makes the activation spectrum above 0.016% supersaturation accessible. The author is aware of only one other such study (Robinson and Scott, 1981) which indicates that this time is over estimated and may be as short as 120 seconds. This discrepancy will also be addressed in Chapter 5

Of primary concern in design and construction of an IHC is then the supply of water vapor, maintenance of 100% relative humidity and a sufficient flow and velocity profile to assure the required residence time.

2.2.1 Laktionov Chamber. Laktionov (1972) chose a logical and simplistic method to design his first isothermal haze chamber at the Institute of Applied Goophysics (IAG). Using a cylindrical TGDCC in a vertical configuration, he simply operated it in an isothermal mode. The chamber was a cylinder of 2 cm diameter and 45 cm high. The sample was introduced in the top and proceeded through the chamber into a particle counter at the bottom. Flow was adjusted to provide a residence time of 186 seconds. Water was introduced at the top and allowed to flow through filter paper down the side of the chamber. Figure 2.2 shows a representation of the IAG chamber.

Literature pertaining to the details of the Laktionov type chamber is scant making a critique of the chamber difficult. However, assuming that Laktionov used standard definitions pertaining to fluid flow characteristics and accurate drawings in the description of his chamber, a major source of error seems apparent. This error arises primarily from the sampling technique and is the result of the flow patterns established inside the chamber. There is no doubt that laminar

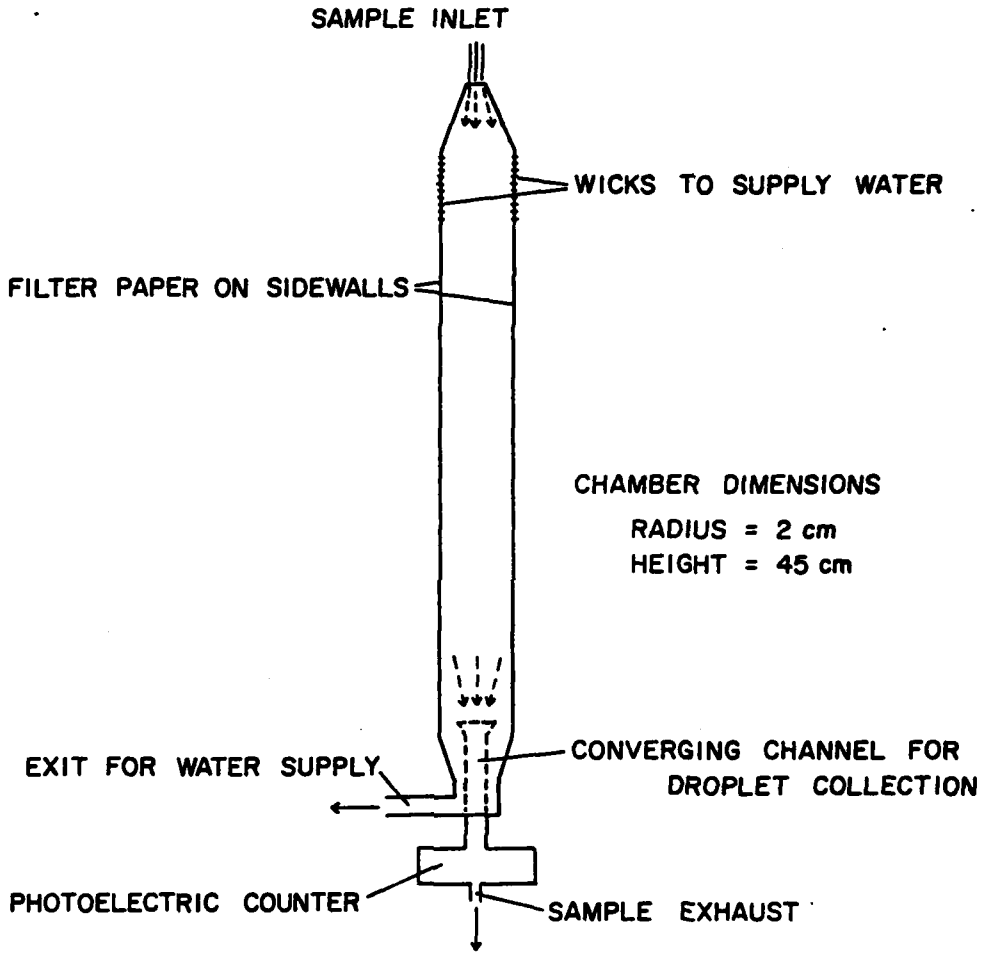

Figure 2.2 Principle diagram of the Institute of Applied Geophysics (IAG) Isothermal Haze Chamber (Laktionov haze chamber).

flow exists in his, and all other chambers, since the Reynolds number is only order of magnitude one. The established flow is a poiseuille type which in a cylinder assumes the shape of a perfectly symmetrical parabola, with the peak exactly in center. Additionally, if a uniform concentration of nuclei is considered, nearly half of these CCN are moving slower than the average speed while again nearly half are moving faster (Bird et al., 1964). Since the entire chamber contents pass into the optical counter this would cause many droplets to experience growth times too short to reach their equilibrium size and thus to be counted as smaller droplets. The resulting droplet size distribution would indicate a supersaturation spectrum with a steeper slope than actually exists.

The Laktionov type chamber has been used in studies of the CCN spectrum primarily by Laktionov (1973) and with slight modification (Hoppel, 1981) by the Naval Research Laboratory (Fitzgerald, 1978; Hoppel, 1979).

2.2.2 University of Missouri, Rolla Chamber. The University of Missouri, Rolla (UMR) chamber (Alofs, 1978) was developed in the same way as the IAG chamber in that it is a TGDCC operated in an isothermal mode. Unlike the IAG chamber, this instrument is rectangular in shape 0.8 cm x 13 cm in cross section and 100 cm high. Sample introduction is also at the top flowing into a photoelectronic counter at the bottom and moisture is supplied by wetted filter paper on the side walls. Figure 2.3 shows the principle diagram for this chamber.

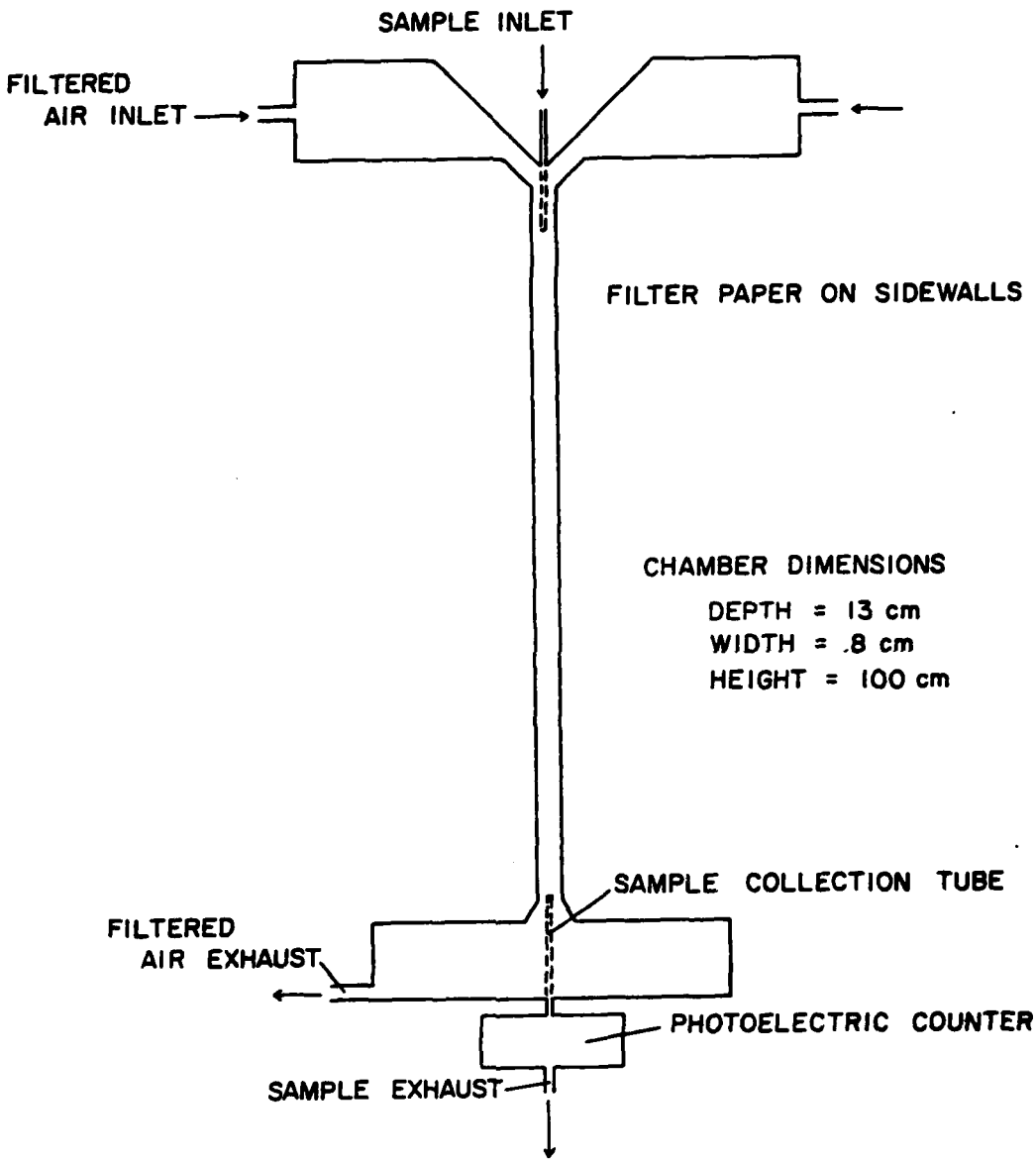

Figure 2.3 Principle diagram of the University of Missouri, Rolla (UMR) Isothermal Haze Chamber.

Two significant improvements are made in this chamber over that of Laktionov. Apparently, Alofs realized the problems associated with velocity gradients across the chamber since his design sheaths the sample in the center with filtered air. The result is a narrow sample stream along the middle of the chamber. The rectangular design of the chamber is also advantageous. Velocity profiles remain parabolic in the chamber, but due to the high aspect ratio (16.25:1) the parabolic flow profile is much flatter than in a cylindrical chamber. These improvements allow for more droplets to be subjected to the same residence time. The UMR chamber was designed to yield a maximum growth time of 200 seconds, slightly higher than that of Laktionov. The growth time was limited by the minimum flow rates acceptable by the photoelectric counter used.

A major disadvantage to this chamber is its excessive height, making it cumbersome for use in aircraft, and it requires excessive support equipment to provide the sheathed air flows into the chamber, such as pumps and filters.

2.2.3 Desert Research Institute Chamber. Hudson (1980) introduced the Desert Research Institute (DRI) cylindrical shaped IHC. This instrument is almost identical in design to Laktionov's differing only in dimensions (150 cm high; 8.9 cm in diameter) and in the method of sample introduction. As in the UMR instrument, Hudson sheathed the sample air flow so that the sample remained centered at the peak of the parabolic flow. In this manner, the residence time of particles can be regulated with great accuracy eliminating the

major deficiency of the Laktionov type instrument. A diagram of this chamber is shown in Figure 2.4.

As in the other type instruments, growth time was limited to 200 seconds due to flow requirements of the optical counter. The major disadvantage of the DRI instrument is the excessive height, required flow equipment and limited residence time. This type of instrument has also been used successfully in field experimentation (Hudson, 1980) and been adapted for aircraft use (Hindman, 1981).

2.3 Reliability and Usefulness of Current Instruments.

As the foregoing discussion indicates, little thought has been devoted to improvements or expansion of IHC's. The DRI instrument is the only one to date to be designed specifically for use as an IHC; the others are merely TGDCC's operated isothermally. All instruments suffer from the same ailment - limited growth time. This deficiency is a direct result of the type of flow used in the chamber and as designed can only be corrected by extending the height of the chamber. Figure 2.5 is a comparison of the velocity profiles in the center of each of the chambers discussed above. The three patterns shown in the figure are drawn to scale based on the dimensions of each chamber and stated growth times.

In order to assess the accuracy of these instruments we must establish operating requirements. We have therefore arbitrarily set a limit of 1% deviation from the expected droplet size upon exit from the chamber. At the longest growth times, and consequently the largest drop sizes, the maximum error from the equilibrium size at

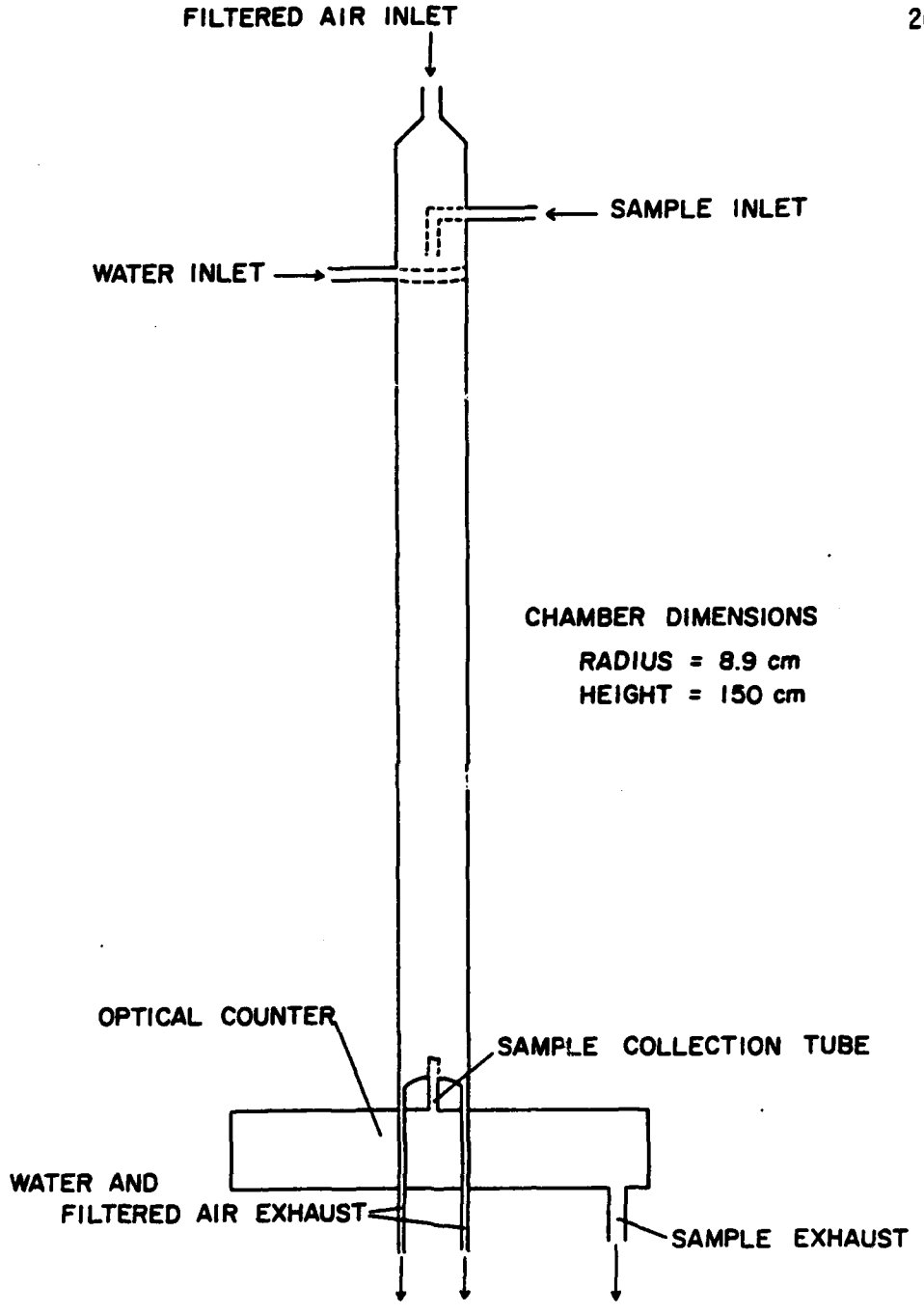

Figure 2.4 Principle diagram of the Desert Research Institute (DRI) Isothermal Haze Chamber.

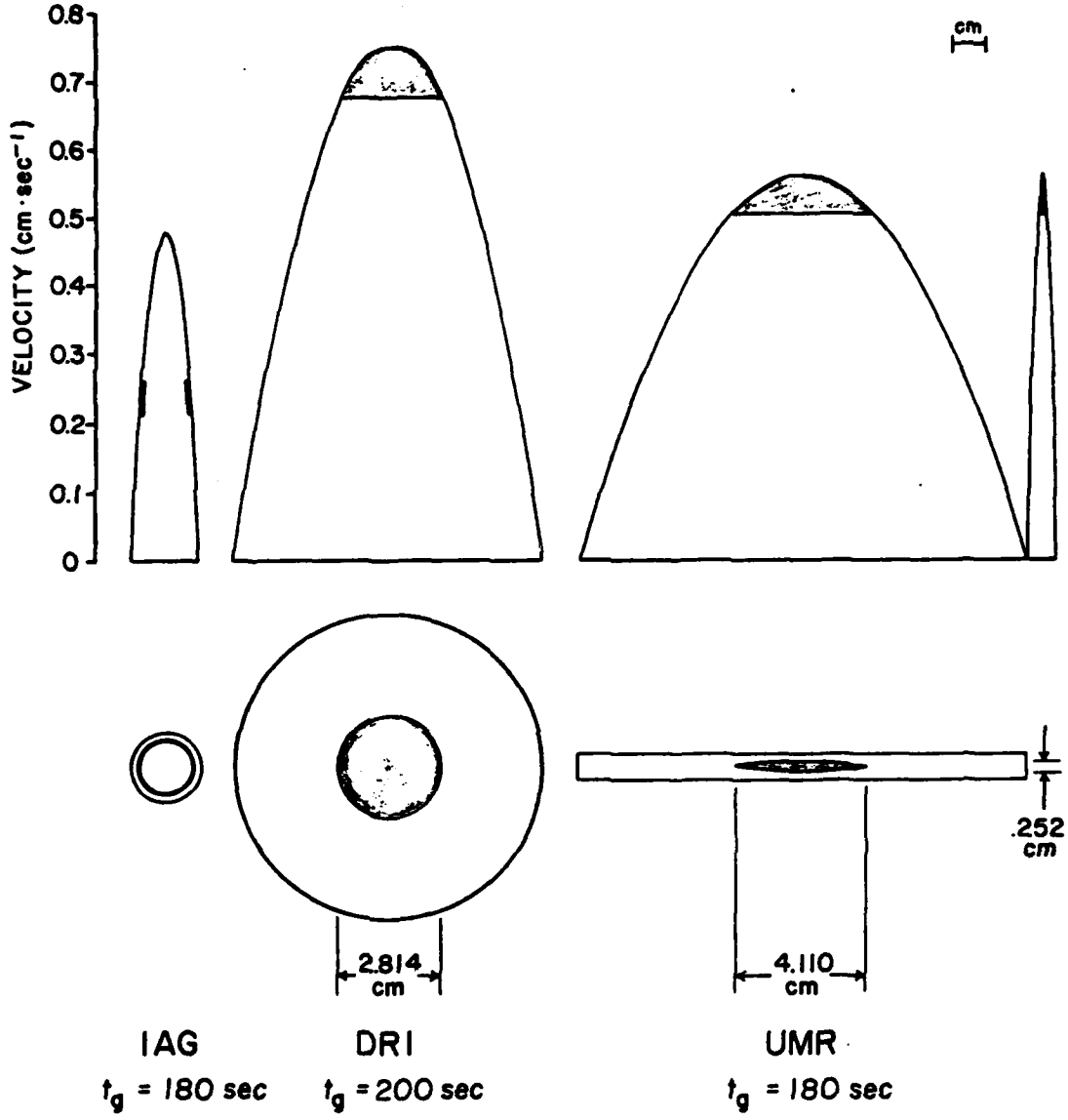

Figure 2.5 Velocity profiles in current IHC's. Shown is the velocity distribution profile across the centerline of each chamber. The shaded portions represent velocity required to produce the stated growth times (t_g) within 10%. The lower portion indicates by shading, the cross sectional area in chambers with t_g ($\pm$ 10%).

100% relative humidity will be 6% with no detectable error for the smallest sizes and shortest growth times. Based on the data compiled by Aleksandrov et al. (1969) this allows a 10% deviation from the required velocity in the chamber. If sampling is accomplished in the region of flow that meets this criteria as indicated by the shaded portions in Figure 2.5 then we can be guaranteed of remaining within an acceptable error margin in the measured size distribution.

It is important to note again that Laktionov based his residence time in the IAG chamber on the average velocity which is only 1/2 that of the maximum. According to the sampling method described by Laktionov (1972) and shown in Figure 2.2, this chamber is entirely unacceptable since 90% of the droplets counted are outside the acceptable region. The reason for the agreement shown in his results for this chamber is that the growth times required for droplets in the overlapping region of TGDCC's and IHC's is short enough that accurate counts were achieved.

In the other two chambers shown, the sampling tube to optical counter must be no larger than the shaded area in the lower portion of Figure 2.5 in order to stay within the error margin we have established. As indicated in Figure 2.5, this size is 2.8 cm for the DRI chamber and .25 cm for the UMR chamber. These tolerances were held in both chambers.

Aside from these velocity profile considerations, two additional characteristics of the flow contribute to limiting the growth time. The first of these is the flow into the optical counter which must

meet certain minimum flow rates in order to operate properly. Second, the flow in each of these chambers is directed downward. In the case of the largest droplets, their Stokian settling velocity becomes considerable and they are moving at a speed (Friedlander, 1977) 10-30% faster than the air flow, thereby reducing the residence times in the chamber.

It was implied earlier that growth times and data reduction methods may be subject to error and this is discussed in the fifth chapter. Nevertheless, the chambers mentioned here have all used the same growth times and theoretical base and therefore can be compared within these constraints. This was in fact accomplished during the Third International Cloud Condensation Nuclei Workshop at Reno, Nevada in 1980 and the results presented by Fitzgerald et al. (1981). The review shows that there is generally good agreement between the UMR and DRI instruments and that they are sturdy and reliable for use in field experimentation. Most importantly however, is the promising future of isothermal haze chambers, not only in expanding the CCN spectrum but also in studies of fog and haze along with other areas of aerosol science.

2.4 Future of Isothermal Haze Chambers

This study undertaken at the Cloud-Aerosol Interactions Laboratory (CAIL) at North Carolina State University represents an innovative approach at improving the IHC beyond the chamber used by Laktionov ten years ago. The initial goal was to produce an instrument with extremely long growth times but consideration is given to addressing

the future requirements and uses of such an instrument. The result of this research is presented in Chapter 4 and as will be seen, represents a tremendous advance which will expand upon the operating range of current instruments, and also provide a versatility not presently available.

CHAPTER 3

3. MOVING BOUNDARY ISOTHERMAL FOG CHAMBER

3.1 Design Considerations

Instruments used in the study of activation spectra of atmospheric aerosols must be capable of providing an adequate moisture supply and sufficient residence to produce the desired amount of growth. In the case of isothermal haze chambers, the residence time is of primary concern since it provides the mechanism whereby the activation spectrum below 0.1% supersaturation may be studied (Sinnarwalla and Alofs, 1973). Instruments currently in use, and previously described, can only increase residence times by extending the height of the chamber. This is not desirable since it makes the instrument less useful for field studies. Therefore, to make significant improvements, a new instrument must have increased growth times, while at the same time no increase in size.

Real time, in situ measurements is an unquestioned necessity (Saxena and Kassner, 1970; Fukuta and Saxena, 1979a) in modern day cloud physics instrumentation and must be considered in instrument design. This requires a design which is compact, lightweight, easy to maintain and simple. Facility of operation and simple design should not take precedence over reliability and therefore must be carefully considered during the design stage.

As has been previously discussed, the flow characteristics within the chamber are crucial in providing reliable measurements. Laminar flow is essential, but parabolic flow profiles should be avoided

if possible. The reasons for this were delineated in the previous chapter and need no further discussion here. Plug type or perfectly flat flow profiles are preferred and the instrument should be designed around this goal. Continuous flow with homogeneous dispersion of aerosols is also necessary to provide uniform concentrations within the chamber. The type of flow produced in the chamber has been the main source of limitations and criticism of current instruments, so most of the improvements sought in the new chamber are centered around this theme.

Increased residence times in a small chamber imply that direct observation of growing droplets should be easily accomplished and, indeed, desirable. Consideration should therefore be given to providing observation windows and illumination capability inside the chamber. It is also desirable to have the ability to heat or cool the chamber so that the instrument would have tri-modal capability of isothermal haze chamber, TGDCC, and ice thermal diffusion chamber. This tri-modal versatility is not currently available in any instrument and would prove valuable in large scale field studies.

The isothermal haze chamber presented here contains all the design considerations mentioned. In many cases the requirements are fully met. However, some of the considerations required compromise especially in the case of producing plug type flow. Additionally, the time constraints on the project necessitated omission of some requirements such as application and removal of heat from the chamber. However, the design of chamber was arranged so that these could be

incorporated at a later time without major modification. Since we realized that expansion of the project was feasible in time, the approach was to design a prototype which operates as an isothermal chamber only, providing growth times and reliability not available in current instruments, but portable and easy to maintain.

3.2 Design and Construction

The entire design and final construction of the instrument was conducted at the Cloud-Aerosol Interactions Laboratory (CAIL). Because of the need for extreme precision and tolerances, fabrication of components was done by the Physical and Mathematical Sciences machine shop at North Carolina State University. Their workmanship and precision proved to be superb and contributed greatly to the success of the new instrument. The supporting framework of the instrument is constructed of 1/4" acrylic, chosen for its light weight, transparency and thermal insulating properties. The chamber itself is constructed of aluminum. The two larger walls are 1/8" thick while the smaller walls are 1/4" thick, one of which is replaceable by clear acrylic. Aluminum was chosen for the chamber since it is also lightweight, but thermally conductive and more rigid than acrylic. Since this prototype is operated isothermally at ambient temperatures, higher conductive material such as copper was not considered necessary. Stainless steel is used in other parts of the instrument because of its non-corrosive ability and ornamental appearance while the sample induction device is made of brass. A sectional view of the entire instrument is shown in Figure 3.1 for reference, while Figure 3.2 is a photograph of the fully assembled instrument.

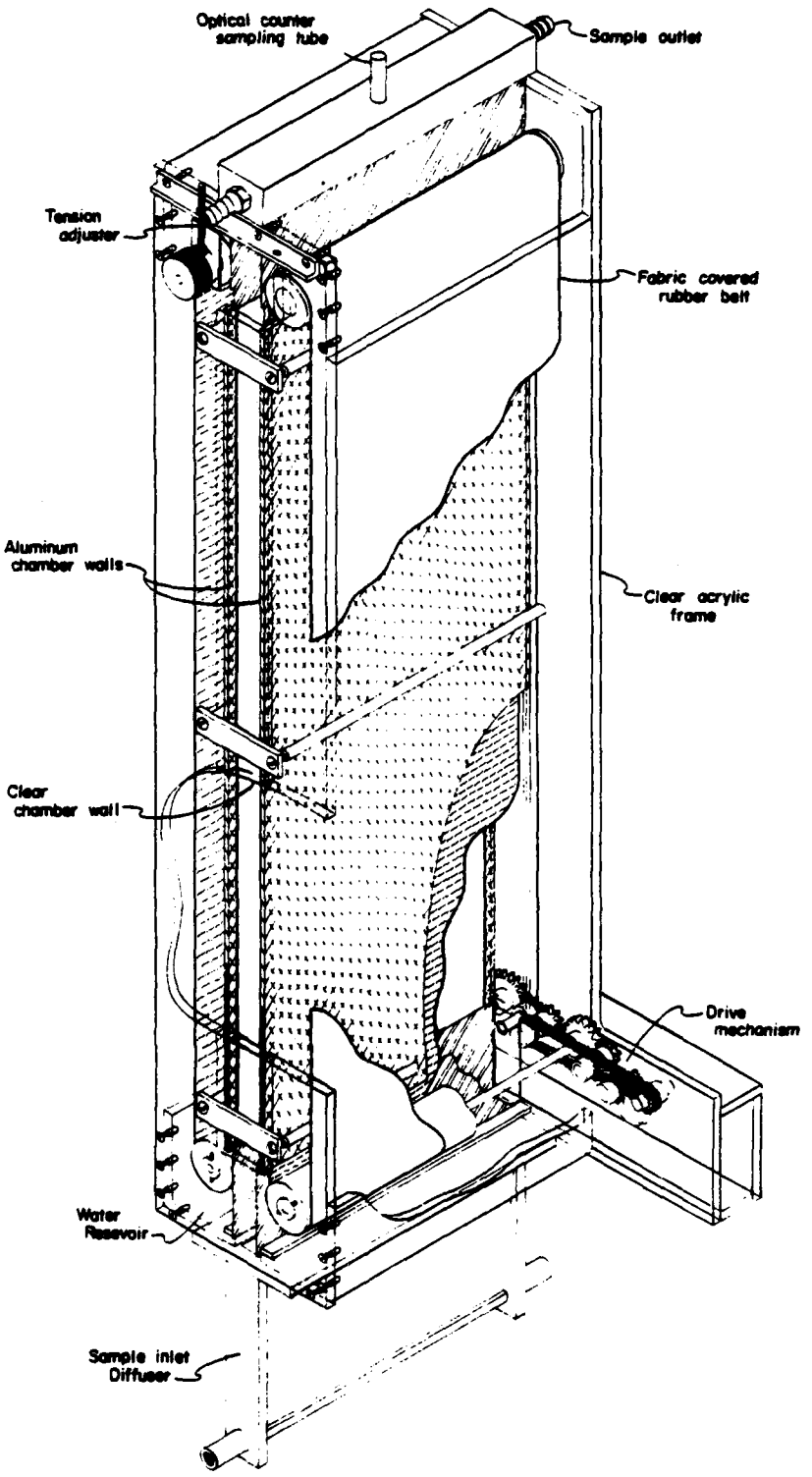

Figure 3.1 Sectional cut-away view of MOBIFOC.

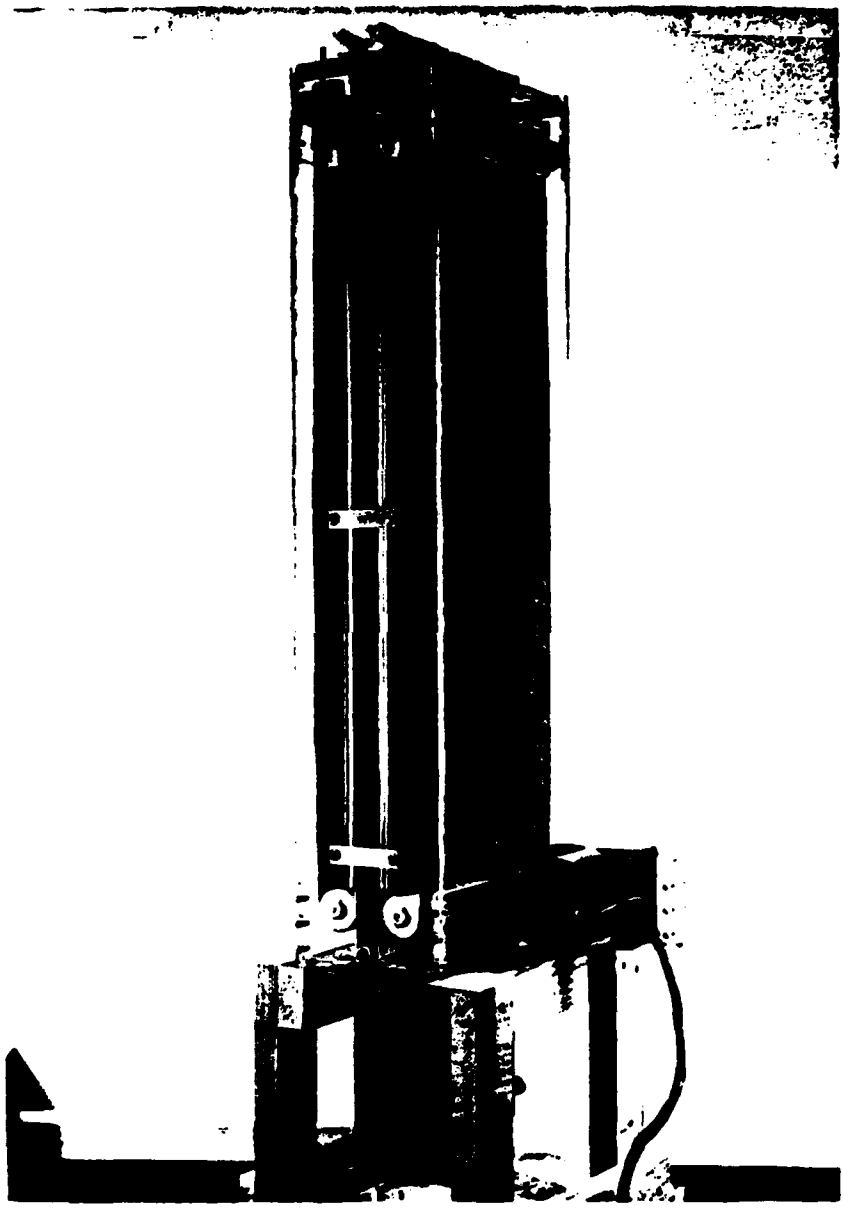

Figure 3.2 Photograph of fully assembled chamber.

3.2.1 Chamber Size. The main part of any isothermal haze chamber is naturally the chamber itself where the droplets are grown, the remainder of instrument being necessary to the introduction and measurement of sample or to the maintenance of the chamber environment. Clearly, the chamber is the first step in the design of a new instrument. We desired to produce a long growth time without extending the height of the chamber and the obvious initial solution is to reverse the downward flow of current instruments to upward flow to counteract gravitational acceleration and settling. We therefore wished to see the effect on residence time of a growing droplet in a limited height with upward flow. Two factors must first be examined in order to determine the chamber shape and design. These are the growth times to final size of droplets and flow rate through the chamber. Using the operating extremes of previously designed IHC's we desire a minimum growth time of 200 seconds which will produce a droplet of about 2.5μ radius (Laktionov, 1972; Alofs, 1978; Hudson, 1980). This growth time must be accomplished in a chamber of no more than 50 cm in height. The chamber shape was to be rectangular since this allowed for ease of fabrication, installation of observation windows and later application of temperature gradients which would be difficult with a cylindrical shape. The dimensions of the chamber were determined to be 2 cm deep by 20 cm wide by 50 cm high. The depth and width were chosen out of convenience. The aspect ratio (width:depth) and dimensions are nearly identical to those used by Fukuta and Saxena (1979a) and therefore several parameters which were necessary to derive in our new chamber have already been theoretically

and experimentally determined. From the results presented by Saxena and Kassner (1970), Fukuta and Saxena (1979a,b) and through personal communications with Dr. Saxena it was determined that an additional 8 cm of height would be more than enough to insure full establishment of boundary layer and laminar flow and complete relaxation of the sample to stable equilibrium with the chamber environment. Additionally, Laktionov (1972) has shown that 100% relative humidity is established in the chamber at less than 8 cm except for the very largest of flow rates.

The final chamber height is now 58 cm. This allows for the full 50 cm to be utilized for growth and study of droplets. In order to insure that droplets acquire the proper growth time, the flow rate must be slow enough so that the sample air stream traverses the chamber in the amount of time required, while at the same time, the rate must be fast enough to counteract the terminal fall velocity of the fully grown droplet. Since our requirements are such that we wish to have a minimum growth time of 200 seconds, the time required for growth to about 2.5μ radius, we can now determine the operating limits of our chamber. Using the data presented by Aleksandrov et al. (1969) we determined the time required to grow droplets to at least .95 r_{100} for droplet sizes $2.5\mu \leq r_{100} \leq 5.0\mu$. At the same time, we examined the settling velocity for the same size range as given by Friedlander (1977). Figure 3.3 shows the plot of terminal velocity vs. radius and the speed of air stream to provide the necessary residence and growth time. The point where these two lines intersect determines the upper limit of growth

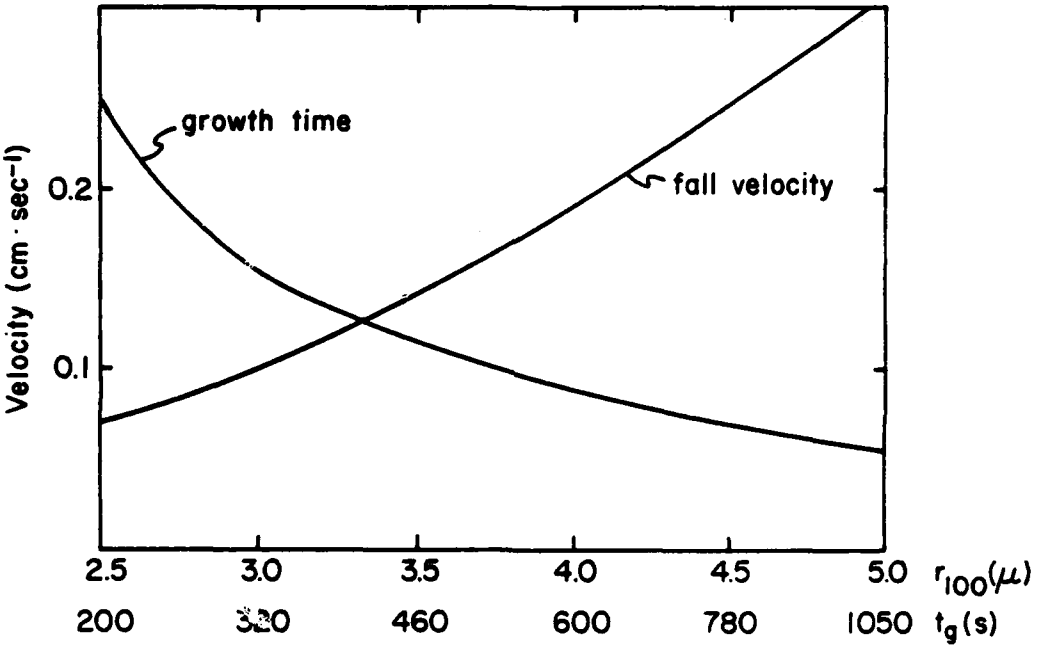

Figure 3.3 Limiting velocity considerations. Fall velocity of droplets in chamber of equilibrium radius, r_{100} and velocity required in chamber to produce the indicated growth time (t_g). The point of intersection indicates steady state operational range in MOBIFOC.

time and residence time of our chamber. As can be seen, this point occurs at $r_{100} = 3.3\mu$ and a residence time of 400 seconds. Therefore, we have managed to double the growth time over existing chambers while operating at a steady flow rate. We also see that by limiting the flow rate so that the air stream velocity is equal to the terminal velocity we are able to suspend droplets of a given size for nearly indefinite periods of time.

The main drawback with operating conditions thus far described is the parabolic velocity profile. As previously noted in the discussion of current instruments, the parabolic profile causes a large difference in droplet growth rates throughout the chamber. Also, since there is a peak velocity in the center, measurement techniques require great precision to insure that sampling tubes are in perfect alignment, which as pointed out by Alofs (1978) is a difficult task. In order to maintain our requirements of simplicity and reliability in this respect, a plug type flow is desirable. Additionally, plug type flow will guarantee all droplets within the chamber are subjected to identical growth times and also allows an environment which more closely resembles natural conditions of haze formation.

Dr. Saxena in personal discussions with the author suggested the possibility of moving chamber sidewalls in an attempt to improve the velocity profiles. The idea was originally conceived in relation to ice crystal nucleation experiments where the large sizes and lower concentrations require more uniform chamber velocities.

In order to determine the velocity profiles resulting from moving sidewalls numerical integration of the equations of motion and continuity are required. Appendix A details the equations and boundary conditions used and the methods of solution. Several solutions were generated for the equations corresponding to different flow rates and velocities both with and without moving boundaries. As expected, the poiseuille type flow (forced flow) due to application of pressure differential between the entrance and exit of chamber and the motion of moving sidewalls is additive. Additionally, from several solutions of equations using different initial conditions we find that so long as the ratio of forced flow velocity to sidewall velocity remains constant, the velocity profile will always remain the same. The additive property of the two flows suggests that plug flow is approached as the forced flow approaches zero. Figures 3.4 and 3.5 show the predicted velocity profiles within the chamber. Part of the testing procedures will include verification of the predicted flow profiles.

3.2.2 Moving Boundary. With the theoretical expectation of plug flow, a practical method of achieving moving boundaries is needed in the design. The idea of using a belt to accomplish this was derived from observing the operation of a belt sander. Two potential problem areas were immediately recognized. The first was that the belt must remain perfectly straight along the entire chamber height to prevent turbulence and directional changes in flow. Second, since one of the chamber design requirements was to allow for application of heat, the belt must be heated or be constructed of a material which is highly

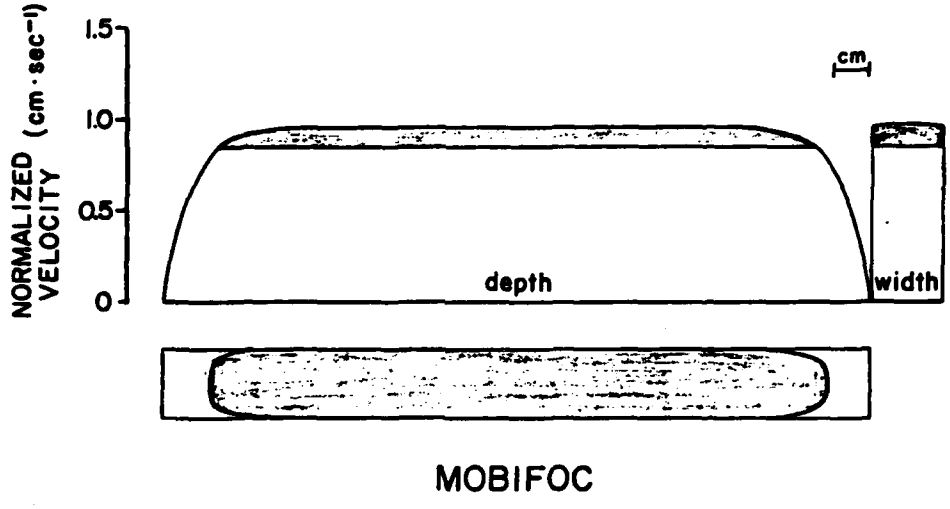

Figure 3.4 Velocity profile in MOBIFOC with moving boundaries. Indicated velocity is normalized to boundary speed. Shaded portion in upper part of figure indicates where velocity is within 10% of that required to produce desired growth time (t_g) while the lower portion indicates the cross sectional area where $t_g \pm 10\%$ is realized. c.f. Figure 2.5.

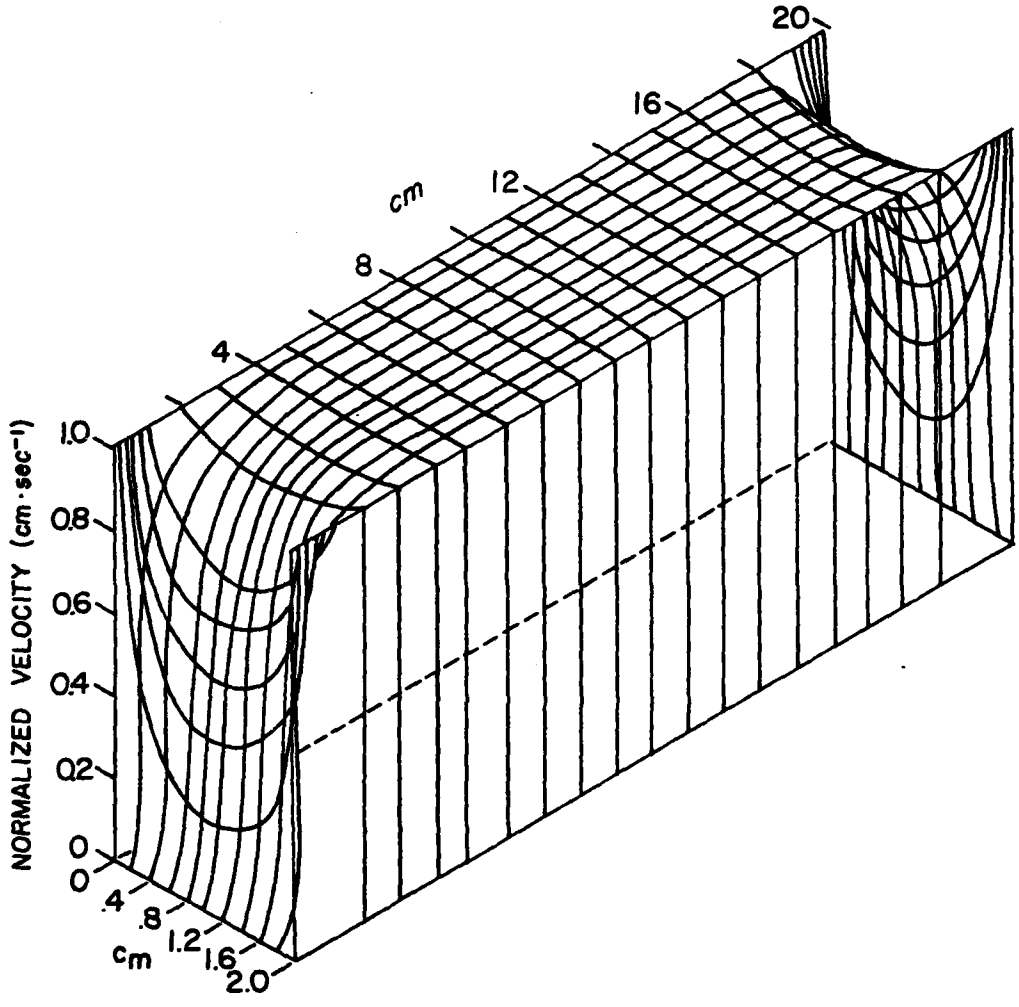

Figure 3.5 Three dimensional velocity profile in MOBIFOC. Velocity profile throughout chamber with moving boundaries indicating nearly plug type flow.

conductive to allow heat to pass through. We opted for a solid metal chamber with the belts passing over the inner walls and constructed of a thermally conductive material. After discussions with the Department of Materials Engineering at North Carolina State University, we decided to try a solid copper belt. Samples of thin copper sheets of various hardness and thickness were tested in our laboratory for flexibility, rigidity and stress. Our tests revealed that copper was not suitable since a sheet flexible enough to be used as a continuous belt would not remain flat and a sheet which would remain flat was not flexible enough to use as a belt. We then tested samples of woven wire mesh belts which were indeed flexible and remained flat and rigid. These belts however need complicated tracking and drive mechanisms, are thick (1/8") and are an extremely expensive special order item. In light of the fact that the instrument designed here is a prototype to be operated in an isothermal mode we decided to delay implementation of this type of belt until after the prototype had been "debugged." Another factor in this decision were warnings during casual conversations with machinists that a belt moving inside a closed chamber with the tight tolerances required would drift and bind causing disruption of constant laminar flow and possible damage to the instrument. Although we were confident this would not be a problem, we thought it wise to use other, less expensive materials until tests could be conducted to determine the amount of drift actually encountered.

Our final choice of belt material was fabric reinforced rubber 1 mm in thickness. One side of the belt is smooth, the other rough which provides good traction on drive roller. The method of driving the belts is similar to that employed in a belt sander. Two rollers are used for each belt, one above the chamber and one below. The rollers are constructed of delryn 3.2 cm in diameter. The top roller acts as an idler and rotates around a 6.4 mm diameter stainless steel shaft. Precision ball bearings are pressed onto shaft and into rollers to provide as friction free mechanism as possible. The shafts extend beyond the instrument sides and are equipped with adjusters and lock nuts.

The adjusters serve two functions. The first is to maintain tension in the belt so it does not slip around the rollers and the second is to align the rollers by raising or lowering one side of the belt so that the top and bottom rollers are parallel and belt will not drift to one side. The lock nuts screw onto the stainless steel shafts. The framework in which the rollers rest is slotted for adjustment and therefore is a source of leaks into the instrument and chamber. Gaskets were hand made in our laboratory from silicon caulking compound and large flat washers were fabricated from heavy gauge steel. The lock nuts therefore serve two functions also: they lock adjustments so they remain fixed and they also tighten against the washers so that gaskets are compressed to insure an airtight seal around rollers. The assembled idler roller, belt and gaskets can be seen in Figures 3.1 and 3.2.

The bottom rollers serve as the drive mechanism for the belt. The belt is driven by friction caused by tension on the belt. The bottom rollers are also constructed of delryn and of the same size as the idler rollers on top. The main difference from the top rollers is that the bottom is pressed onto a stainless steel shaft also 6.4 mm in diameter. Roll pins are inserted in the front side of shaft and countersunk into the end of the roller. The roller and shaft are locked to each other and the shaft extends outside the rear of instrument where the roller and shaft are both driven by a gear assembly. The bottom roller and shaft both reside in a water reservoir located below the chamber. The use of metallic bearings is not advisable since they would be submerged in water during use and subject to rapid corrosion. The shafts therefore rotate inside teflon bearings which are pressed into the acrylic framework at both ends of the shaft. A teflon bushing is used where the shaft extends through the instrument wall. Figure 3.1 also shows the bottom roller assembly in detail.

3.2.3 Belt Drive Mechanism. Both belts are driven by a single motor which is attached at the rear wall of the instrument. The foregoing discussion of velocity profiles pointed out that a constant profile could be maintained providing that the ratio of forced flow velocity to belt speed remained constant. In order to accomplish this, the belt speed must be adjustable. A variable speed A.C. motor and gear reduction unit are used which provides a final speed of 0 to 26 rpm at the drive shaft. The electronics were placed in a separate box which attaches to the motor with a convenient plug in receptable. Adjustment of speed is accomplished through the use of a vernier, ten

turn potentiometer graduated from 0 to 10 in hundredths. The vernier allows for precision tuning of belt speeds. The drive shaft extends out of the gear reduction unit into the gear assembly mechanism which is enclosed in a clear acrylic box attached onto the outside rear of the instrument frame work. Figures 3.1 and 3.2 show the location of the gear assembly and motor while Figure 3.6 is a close up photograph showing the gear alignment and positioning.

Within the gear assembly, a further gear reduction of 2:1 is achieved. This was done for two reasons. First, we felt that 26 rpm, which translates to nearly 1.5 cmS^{-1} was much faster than we needed and secondly the gear reduction allows for greater control. The gears which perform the reduction are all 12 teeth 24 pitch pin hub spur gears. There are a total of five of these. Two are attached to the shafts which drive rollers and have a one inch pitch diameter. Both of these are made of aluminum. In Figure 3.6a we can see that the roller gear on right is driven by two smaller gears of one half inch pitch diameter and the left roller gear is driven by only one. This allows for only one motor to drive both rollers, but in opposite directions so that both belts move in the same direction at the same speed. The smaller gears which mesh with the roller gears are made of stainless steel while the remaining small gear is made of aluminum. The different materials provide for longer life and quieter operation. The photograph in Figure 3.6b shows that these gears are positioned at the very end of the shafts on which they are placed. The inner part of the shafts are used for connection to motor drive shaft.

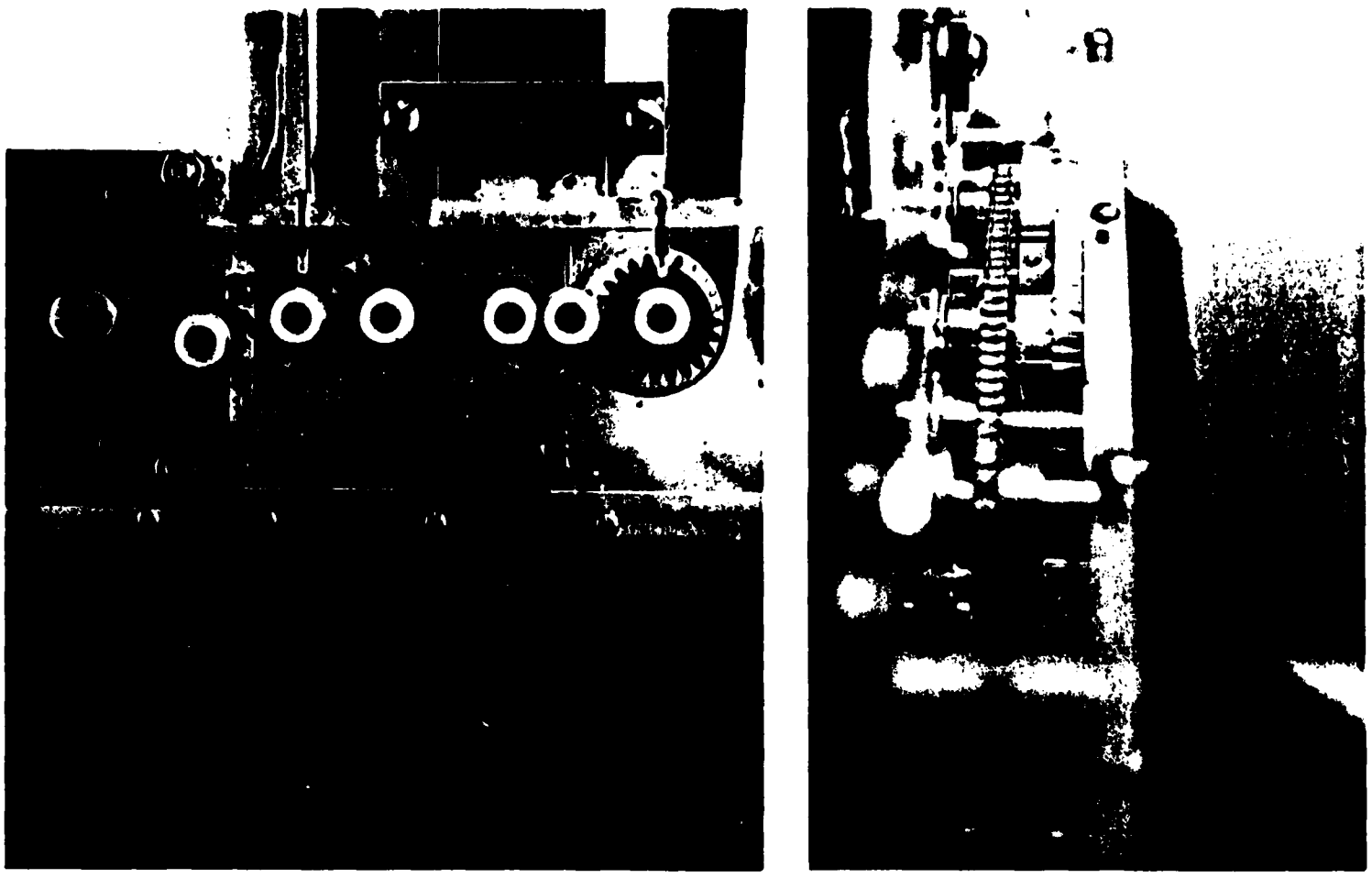

(a) (b)

Figure 3.6 Photograph of belt drive gear assembly mechanism. (a) gear and drive chain alignment; (b) gear positioning

The figures show that a chain and sprockets are used for the drive mechanism. The original design did not call for this but instead a "no-slip" drive belt and geared pulleys were used. When the instrument was first assembled, we noticed that at high speed and under tight tension of moving boundaries, the "no-slip" drive belt had a tendency to slip and cause spasmodic motion of one of the moving sidewalls. The belt broke shortly thereafter and we decided that the use of a miniature chain and sprockets would provide greater reliability. The CAIL has another instrument which utilizes this same arrangement of belt and pulleys and we have found that breakage occurs often because of deterioration of the belt materials. The sudden pre-mature breakage of the belt in this instrument may have been due to misalignment of the pulleys, but we feel more secure with the current arrangement of chain and sprockets. The sprockets are all 12 teeth one half inch pitch diameter sprockets and manufactured of stainless steel. There are a total of four. One is attached to the motor drive shaft and one each is on the same shaft as the 1/2 inch spur gears which drive the roller gears. The fourth is an idler sprocket which reduces the slack in chain. Adjustment of the chain is accomplished by sliding the motor horizontally in adjustment slots provided in the frame. Each gear and sprocket is mounted on a stainless steel shaft of 1/4" diameter by use of set screws and flats milled in the shaft. With the exception of the roller shafts which have been previously explained and the motor shaft which is self contained, all the shafts rotate in teflon bearings which are pressed into the walls of the gear assembly housing.

3.2.4 Final Chamber Design. We have already discussed the establishment of the chamber dimensions and the means and operation of moving sidewalls. These must now be integrated into a single unit which will finalize the chamber itself. In order to grow droplets in the chamber, we must have a means of supplying moisture to the chamber. In the chambers currently in use, water is supplied at the top and allowed to flow continually with gravity to the bottom thereby maintaining a moisture supply to the walls at all times. In our chamber with the belts moving upward this arrangement is not possible. It also complicates the design because a source reservoir and a catch basin at the bottom are needed. We decided that coating walls with a highly absorbent material would serve our purpose. Ordinarly, filter paper is used for this purpose but we planned to take photographs inside the chamber and would require a dark field, preferably black. We were unable to locate black filter paper and decided to try fabric. We knew that water would be supplied to the belts by a reservoir through which the belt passed so we needed a material which had a high rate of absorption and a long retention time after saturation. Several fabrics were tested for the above characteristics. The tests consisted of submerging the material in water for a few seconds then hanging them up to see how long they retained the absorbed water. The best material found was Pellon, an interfacing material used in the clothing industry. Black, medium weight Pellon was glued to the rubber belts and rear chamber wall. Since photography and observation were desired a clear wall was used in the front and left uncovered.

The sidewalls of the chamber were constructed of sheet aluminum 20.6 cm by 58 cm by .32 cm thick. These are simple flat plates milled to the precise dimensions. The fabric covered belt is 20 cm wide and moves upward inside this aluminum wall, and in effect, becomes the wall itself during operation. A clearance of .25 mm is allowed between the belt and aluminum wall and on either side of the belt. Since viewing is impossible through the opaque belt and it is convenient to consider observation as taking place from the front, the large walls with moving boundaries are called the sides and the clear wall is called the front. The back and front walls are each 1/4" thick since this will rest in the framework which is also the same thickness. Three of these walls have actually been constructed. Two are of aluminum and the third is of clear acrylic which is used when observation is desired. For the duration of construction and testing, the clear wall has been used in the front. The front and rear walls are identical in design. They are 3.9 cm wide and 58 cm high and are slotted .3 cm deep so that the sidewalls will interlock to form a rectangular chamber. The bottom of this slot contains an "O"-ring seal to prevent leakage at the sides. The slots are positioned so that the distance between the belts is 2 cm. The entire chamber including the belt assembly then rests inside a supporting framework so that it is essentially independent of the rest of the instrument. A cutaway sectional view of the chamber is shown in Figure 3.1.

3.2.5 Framework. The framework of the instrument actually supports the chamber and moving boundaries assembly and also serves as a housing for other parts necessary to maintain flow and environment in the chamber. Clear acrylic is the material used for construction. One of its advantages as a building material is the ability to form by heating and bending. Except for mounting the motor and gear reduction unit on the side, the framework may be made completely symmetrical. This reduces the manufacturing cost while at the same time simplifying the design. Water is supplied to the chamber by allowing the belts to pass through a water reservoir as it moves over the lower rollers. Separate reservoirs are used for each belt so that different solutions may be used for each belt similar to the method of operation of a chemical gradient diffusion cloud chamber and for thermal separation when temperature gradients are applied. The separation of the two reservoirs also allows for unhindered air flow directly into the chamber between the reservoirs. One-thirty second inch stainless steel dividers are used on the inside of the reservoir to prevent the water from leaking out. There is a separation of nearly 2 cm between the dividers so that they also serve as an induction device for air flowing into the chamber. The reservoirs are 6.5 cm deep and the water level is kept high enough so that at least half of the bottom roller is submerged at all times insuring generous soaking of the felt covering.

Nearly a mirror image of the water reservoirs is employed at the top of the framework above the chamber. Stainless steel dividers are used here also serving as an extension of the chamber so that the flow remains laminar after exiting the chamber. The front and rear of the frame assembly are flat rectangular pieces which forms the other two sides of the reservoirs. These pieces forming the front and back of the instrument are slotted on the inside at the top and bottom so that the aforementioned stainless steel dividers fit into these slots and help maintain their position and prevent leakage of air and water. These pieces also house the teflon bearings on lower rollers and have adjustment slots where the top roller shafts are locked into place. A hole is cut into the center the same size and shape as the chamber front and rear walls. The four chamber walls then rest inside this opening so that it is suspended in the center of the acrylic framework. The entire framework when assembled as in Figure 3.1 and 3.2 forms a rectangular box 71 cm high, 13 cm wide and 21 cm deep with openings at top and bottom the same size as the chamber. In the center the supporting frame is therefore an extension of the chamber itself.

Because acrylic is so flexible, three stainless steel spacers are placed along the height at the top, bottom and middle of the chamber. These are exactly 20 cm long and pass between the front and back frame supports outside the chamber, but inside the outer edge of the rubber belt. Across the outside front and back of chamber a rigid brace is placed. The spacers are threaded in the center and the braces are screwed into the spacer thereby preventing the framework from flexing

when assembled. The braces at the same time place pressure on the chamber walls which compresses the "O"-ring thereby insuring an airtight chamber and bolting the chamber in place in the framework. Figures 3.1 and 3.2 show the braces and spacers in position. The entire framework and chamber when assembled is surprisingly sturdy so that mobility is achieved without danger of losing reliability.

The side, top and bottom pieces have threads tapped into the acrylic and is screwed together from the front and back. The front side utilizes helicoil inserts in the acrylic so that maintenance can be performed without damage to the threads. Two major disadvantages exist with using acrylic as a construction material. The first is the softness if tapped threads are used. The use of helicoil inserts reduces this problem, but overtightening of screws can still cause irreparable damage. The second problem is that acrylic will break or crack if it receives a sharp blow. The choice of acrylic is therefore one area of compromise in our design. We sacrificed some strength in building materials for the advantages of light weight, aesthetics, and expense. However, if a normal amount of caution is used in assembly and handling, this sacrifice is neglible.

3.2.6 Flow System. Sample introduction is achieved through the use of a diffuser which is bolted to the bottom of the frame through the reservoirs. This allows for homogeneous dispersion of sample into the chamber. A rubber gasket is used in the connection to prevent leakage of air and water. Fortunately, thorough testing of size and shape of the diffuser had been conducted by Fukuta and Saxena (1979a)

and we needed only to duplicate their design. We used 1/8" brass in the construction of the diffuser which is a low angle wedge shape 20 cm wide and tapering from 2 to .05 cm at the entrance edge. A 3/8" brass pipe connects across the narrow edge so that sample is drawn into each side of the diffuser. After the air is fully diffused it exits the diffuser and passes between the stainless steel dividers of the reservoirs and then enters the chamber proper. After allowing for up to 8 cm relaxation distance, final flow is established and continues until it exits the chamber at the top passing between the stainless steel dividers. The air is then exhausted through the front and rear of a cap which is placed over the top opening of the instrument and shown in Figure 3.1. This cap is filled with tightly packed foam rubber so that a resistance is offered to the flow and uniform suction is applied across the entire cross sectional area of the chamber. The forced flow is produced by use of a vacuum pump and regulated through a flow meter. The induced flow is produced by the moving boundary assembly as discussed above and in Appendix A.

The droplet counting and detection system is commercially produced by Climet and consists of a CI-208 particle detection system. The flow through this system is much higher than in the chamber, so a CI-294 dilution system is employed to insure isokinetic sampling. The dilution system draws filtered air from outside the chamber and sheaths the sample air drawn from the chamber so that the actual sample flow rate remains constant within the bounds of the main chamber flow rate. Sampling is accomplished through the use of a copper sampling tube which extends through the center of the top cap along the central

axis of the chamber. The entrance of the sampling tube extends 3 cm into the top of chamber to eliminate turbulent effects caused by exit of flow from chamber. A short piece of tygon tubing connects the sampling tube directly to the optical detection system of the CI-208.

3.3 Final Assembly

Because this instrument is designed to study the activation spectrum in the region where fog droplets are formed and since moving boundaries are used in the establishment of velocity profiles we call the instrument a Moving Boundary Isothermal Fog Chamber or MOBIFOC for short. Figure 3.1 is a sectional view of the assembled chamber while Figures 3.2 and 3.7 show photographs of the totally assembled instrument. Figure 3.7b shows the configuration necessary under actual operation. Also shown in Figure 3.7b is the motor control box and the Climet CI-294 aerosol dilution system. Assembly of the instrument is fairly simple although due caution must be used to prevent stripping of threads and breakage.

The assembly procedure involves installing the aluminum chamber into the rear framework support, installing rollers and belts and then connecting the remainder of frame support and braces. Total assembly time is approximately 45 minutes. Unless modification of components is required, there is no need for full disassembly again since the removal of front frame support exposes all moving parts and chamber for maintenance.

3.4 Operation

The chamber is now ready for operation. The motor is plugged into the control box and the speed control set on a low number such as 1 or

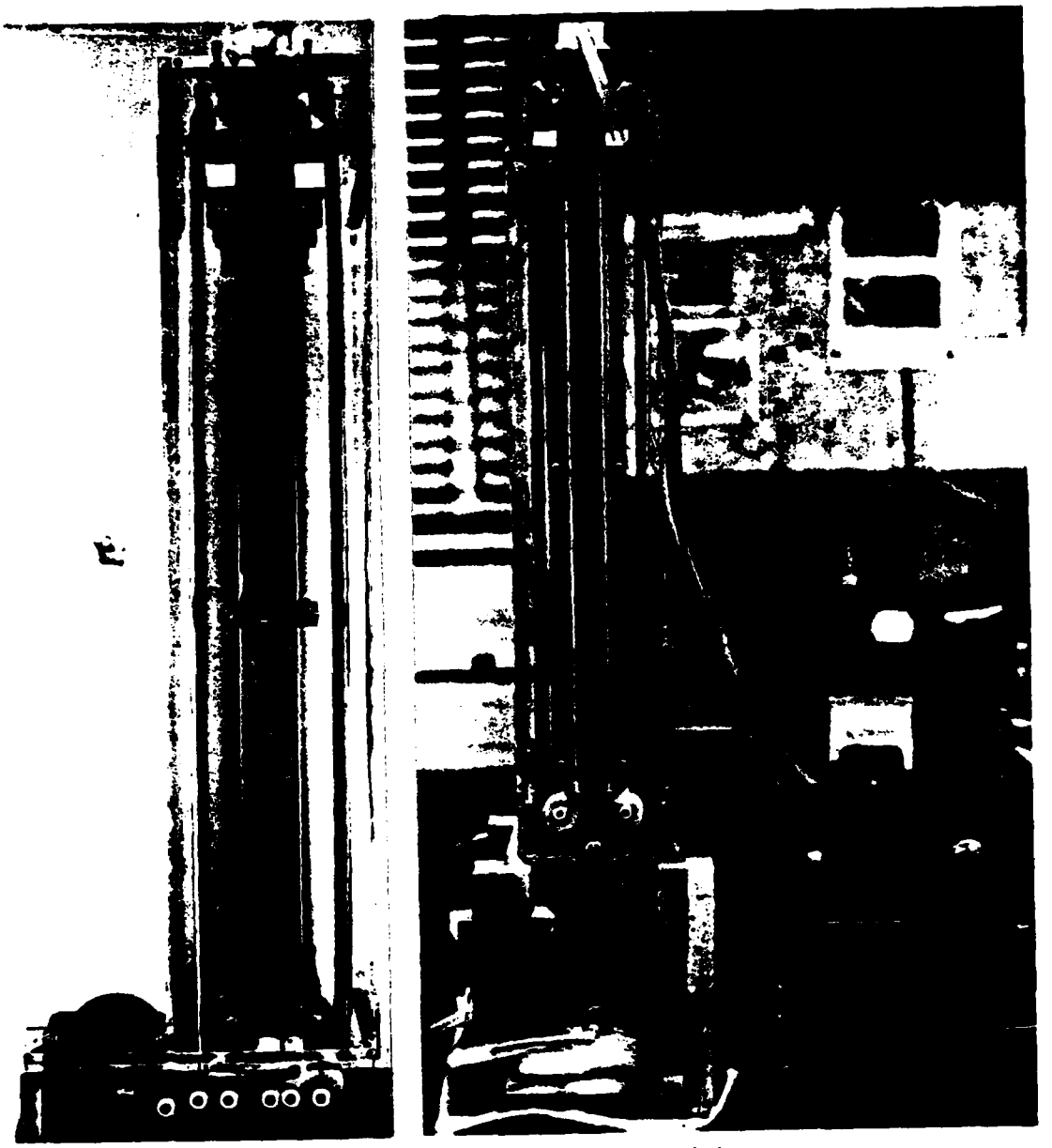

(a) (b)

Figure 3.7 Photograph of fully assembled instrument. (a) rear view; (b) operating configuration with motor speed control box, intake and exhaust hoses and Climet CI-294 dilution system connected.

2. Checking to insure that belts are tight enough to move, water can now be added. We add water to the reservoirs by using a syringe with a flexible tube and insert this through a hole located in the front between the two reservoirs. This can be seen in Figure 3.2 just above the diffuser and below the rollers. The tube on syringe is placed just above the stainless steel dividers and water placed between the belt and divider into the reservoir. This is a slow and cumbersome method of filling the reservoirs. We plan a modification where the filler hole enters directly into each reservoir on the side. This will allow for drainage of the reservoir also, when not in use. Water must be continually added until the belt becomes completely saturated and the water level covers at least the bottom half of rollers.

The belts may now be finally adjusted and locked in place and chamber checked for leaks before operation. To test if the instrument is totally sealed, we place the sample intake into a beaker of water and apply a very slow flow rate to the instrument. If all leaks are sealed, water is drawn into the tube.

The operating conditions such as flow rates and belt speed depend upon the use desired of the instrument. For example, if we wish to suspend droplets for observation then the belt and flow are adjusted for plug type flow with a velocity equal to the fall velocity of the droplets we wish to study. If a supersaturation spectrum is desired, then the flow is adjusted to count and size all droplets of a given size and smaller. Details of settings and calibrations are contained in the following chapter.

CHAPTER 4

4. CALIBRATION AND EXPERIMENTAL RESULTS

Upon completion of MOBIFOC, certain tests had to be conducted to determine the suitability of materials and design. Once suitability was determined and corrections made, experiments were conducted to verify that the established design requirements are met.

4.1 Equipment and Materials Tests

4.1.1 Moving Boundary. The implementation of a moving boundary in an instrument of this type is an entirely new concept which has never been successfully attempted. It is therefore the most significant feature of MOBIFOC and comprises the first tests conducted on the instrument. Our initial concern has already been mentioned which is the possibility of drifting and binding of the belts. To test this possibility we operated the moving belts for long periods of time at various speeds. We immediately found that the belt would bind and slip on the drive roller, but always at the same position. Close examination revealed a defect in the belt manufacture. The manufacturer had been supplied with the tolerances we required, but these were not adhered to. The belt width exceeded our tolerances by a millimeter or more in some spots and it was these locations which were binding between the front and rear frame supports. We trimmed the belt using a sharp knife and after reinstallation had no further problems with binding. There is evidence on the acrylic framework that the belt is drifting to the side and scraping on the acrylic walls, however, the speed of the belt is so slow and the clearance so small that there is no evidence

that the operation of the chamber is affected. We later noticed that the belt had a tendency at times to curve inward at the rear wall of the chamber which indicated that the clearance was insufficient. Since the inside dimensions of the chamber are exactly the same as those of the framework we could not understand why this occurred inside the chamber and not in the frame. MOBIFOC was partially disassembled and after removal of the belts and sidewalls we noticed that the chamber was misaligned in the frame, with the rear wall extending into the framework by about a millimeter, but was flush on the outside. Using a micrometer, we found that the thickness of the acrylic is less than that of the aluminum wall. When the chamber was placed in the framework and the rear braces tightened this caused the whole chamber to be displaced toward the front enough to cause the belt to deflect along the rear wall. This problem was easily solved by using thin copper spacers in between the braces and the outside of the framework. Upon reassembly, with this modification no further problems were encountered with misalignment of the chamber. There is one other problem with the rubber belt resulting from the vulcanized connection. At the point where the belt was joined together, there is a slight bowing outward of the edges so that inside the chamber they are no longer 2 cm apart at this point. If one looks closely at Figure 3.7a this bend can be seen in the belt on the right of the picture. We found two ways to eliminate this. The first is to not only place extreme tension on the belt, but to stretch it and force the belt straight. We feel this places too much strain on the drive mechanism

and so opted for the second solution. This consisted of placing guides inside the chamber which hold the belt against the edges of the chamber walls. The center of the belt is no problem and remains flat at all times. This solution reduces the chamber dimensions slightly, but is of no significant consequence.

4.1.2 Water Supply. The installation of moving boundaries prohibits the use of the conventional method of allowing water to drain down the sides to provide moisture for humidity maintenance. We therefore use an unconventional approach of reservoirs through which the belt passes and becomes saturated carrying the water with it through the chamber.

The Pellon remained totally saturated throughout the chamber regardless of belt speed. A minor problem occurred when the Pellon shrunk and separated from the belt. We attempted to pre-shrink the material by wetting and drying with a hand held heat gun, but this was apparently inadequate. Some spot glueing corrected the problem.

4.2 Calibration Procedures

4.2.1 Moving Boundary Speed. Calibration of MOBIFOC is fairly straightforward and simple. The first set of calibration data gathered was to calibrate the ten turn potentiometer setting to linear velocity of the moving sidewall. This was conducted in the following manner. Guide marks were placed on the belt and a scale placed along side the moving belt. Using a digital stop watch graduated in 100th's of a second the time needed to travel 10 cm was measured. A total of ten measurements for each of the ten major divisions on the speed control was taken and the average for each setting was taken to determine the

speed. The margin of error in the speed setting ranges from 0.6% at 1 to 1.5% at 10 with the largest error only .01 cms^{-1} at the largest setting. Figure 4.1 gives the speed control calibration curve for the belts.

4.2.2 Flow Speed. Similar calibrations are also needed for the flow meter. The particular flow meter used is manufactured by Gilmont instruments and has interchangeable f[illegible] tubes which allow various ranges of flow within the same meter. We chose a range which would provide velocities compatible with the belt speed. The velocity in the chamber is determined by dividing the cross sectional area into the volume flow rate. Since the flow meter is calibrated at the factory, we combine this with the calibration curves furnished by the manufacturer to get the proper calibration curve for our chamber as shown in Figure 4.2.

4.2.3 Plug Flow Calibration and Residence Time. Based on our expectation of plug type flow, with a one to one ratio of flow speed to belt speed, we can combine the two calibration curves given in Figures 4.1 and 4.2. The resulting curve, shown in Figure 4.3, gives the operator the proper settings to use for establishing plug flow in the chamber at any velocity. Since the residence time is easily found by dividing the chamber height of 50 cm by the flow speed, this is also shown in the figure.

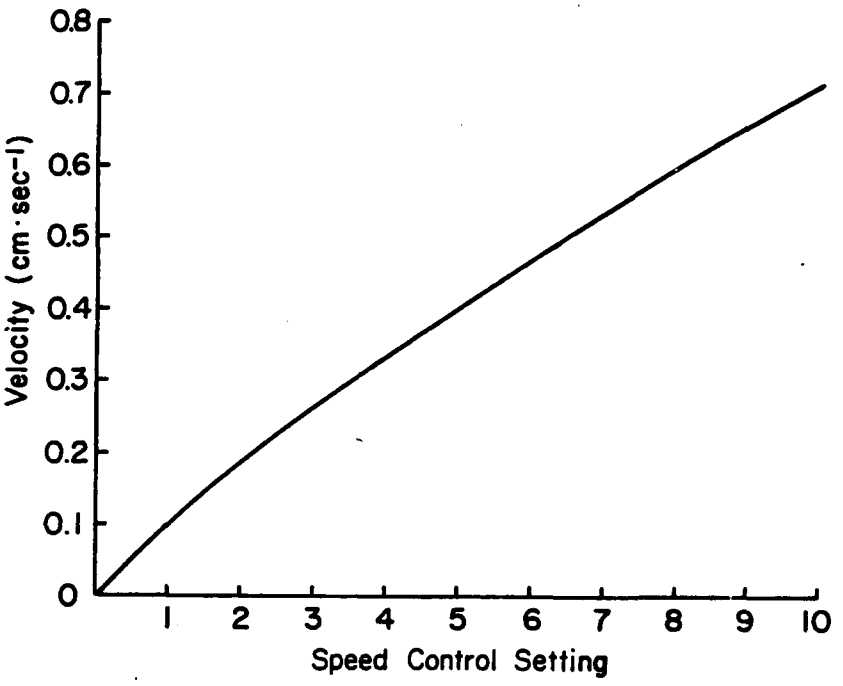

Figure 4.1 Calibration curve for speed control potentiometer.

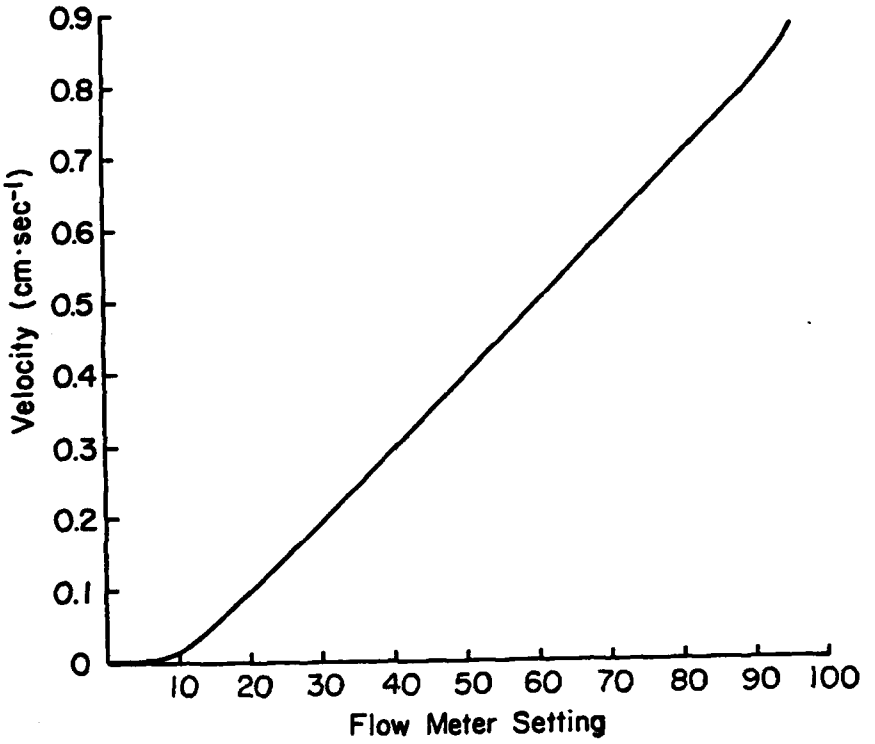

Figure 4.2 Calibration curve for flow meter.

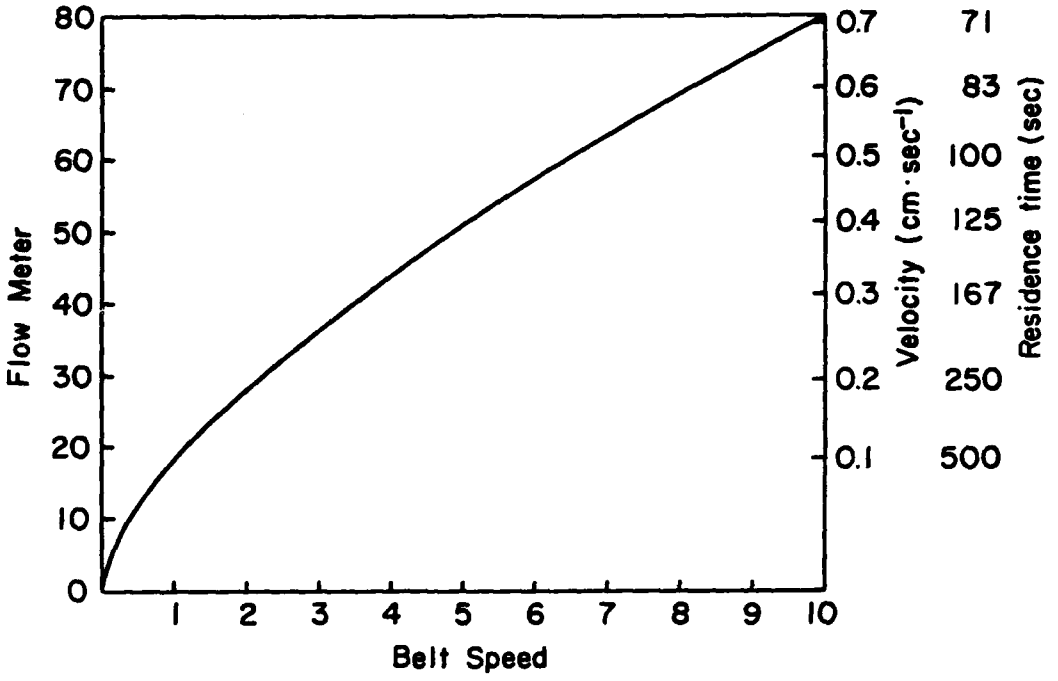

Figure 4.3 Calibration curve for plug type flow. Curve indicates settings on flow meter and belt speed control to produce the velocities and residence time indicated on right hand side of figure.

4.3 Operational Tests

4.3.1 Chamber Flow. Tests to determine the stablity of flow in the chamber and velocity profiles were conducted using smoke as a tracer. Titanium Tetra-Chloride ($TiCl_4$) was used as the smoke tracer. The smoke was introduced into the chamber by saturating a cotton swab in liquid $TiCl_4$ and inserting it directly into a hose connected to the diffuser inlet through a "T" fitting. This insured a constant flow of smoke into the chamber. With the front viewing wall in place it is possible to look directly down into the diffuser to observe the stabilization of the flow after entrance. The smoke enters in a highly turbulent state, but as predicted by Fukuta and Saxena (1979a) the turbulence quickly subsides as the smoke is diffused outward. Within two or three centimeters after entrance, there is no visible evidence of turbulence as the smoke proceeds upward as a smooth laminar unit. Parabolic flow was plainly evident as the smoke proceeded between the water reservoirs prior to entering the chamber.

Titanium Tetra-Chloride produces a very dense smoke which makes it easy to observe and photograph. However, it is also quite heavy and because of this, we could not test the flow profiles at lowest flow rates because the smoke would settle to bottom of chamber. The majority of these tests were therefore conducted at flow meter settings between 30 and 60 corresponding to velocities of 0.2 and 0.5 cmS^{-1}.

The first tests conducted were strictly observations of various flow conditions. We noticed that with stationary sidewalls, the parabolic flow was well established at the entrance to chamber and

continued on past the exit. The disadvantages of parabolic flow are well dramatized in our observations. The velocity shear across the chamber creates a long residence time near the chamber walls. Because of the density of $TiCl_4$ smoke particles, coagulation would occur at the outer edges of flow. Large particles would form and begin to fall. As they fell, they would collide with other smoke particles, gain speed and create turbulent eddies in their wake as they fell. The result was large comet-like disruptions in the flow pattern which rotated and eventually broke up due to velocity shear. At high flow rates this was not as obvious since the coagulation time was greatly reduced. The leading edge of the smoke area did not experience these problems.

We then observed the effect of belt motion. This was done by maintaining a constant forced flow and then varying the belt speed to observe the changes in profile of the leading edge of the smoke. In this manner, we were able to verify our assumption that the forced flow and induced flow were additive as used in Appendix A to determine the velocity profiles. As the belt speed was increased from zero, the leading edge of the smoke could be seen to accelerate continually as the belts increased in speed. At the same time, as the belt speed increased to the same speed as the center of the leading edge of the smoke, a plug flow was observed. From Bird et al. (1964) we see that the induced flow velocity by two moving belts is "V" shaped in the absence of any forced flow between them. Once the belt speed becomes greater than the maximum forced flow, the effect is the same as no

forced flow or a negative forced flow between the belts. As we increased the belt speeds beyond the point of plug flow, we begin to see that the additive property causes an inverted parabolic flow with a maximum at the edges of flow and a minimum in the center.

During these tests we were able to produce residence times for the leading edge of the smoke of 20 minutes or longer. This was accomplished by gradually increasing the flow speed under plug flow conditions to compensate any coagulation and subsequent growth of individual smoke particles. This same process will provide for extremely long residence times of growing water droplets.

With some experience in operating MOBIFOC we proceeded to photograph the smoke profiles. The flow meter was set at a constant reading and smoke introduced in the chamber. Photographs were taken with no moving belts, and then the belts speed increased in accordance with our plug flow operating curve in Figure 4.3, and a second photograph taken. The resulting flow patterns are shown in Figure 4.4. These photographs were taken with the flow velocity at .3 cmS^{-1}. Figure 4.4a was with stationary belts and the parabolic profile is evident. A thin stream of smoke particles in the center above the main flow points out the maximum and presents evidence of the laminar flow in the chamber. Figure 4.4b is with the belt speed set at 0.3 cmS^{-1}. The plug flow is easily seen by the flat top on the leading edge of the smoke.

(a) (b)

Figure 4.4 Photographs of smoke tests to verify velocity profiles. (a) stationary belts; (b) moving belts.

4.3.2 Droplet Growth, Suspension, and Residence Time. These tests were conducted to determine if haze droplets could be grown in the chamber. After growth, other tests were conducted to verify growth time and suspension capabilities. The majority of these tests used ammonium sulfate as the aerosol. Aerosol particles were generated using the bubble burst mechanism. This mechanism is the primary mode of production of sea salt aerosol particles and a good explanation of the details may be found in Pruppacher and Klett (1980). The bursting bubble ejects a fine spray of salt solution into the air which breaks up into droplets small enough to remain airborne. Some of the droplets evaporate leaving a salt particle behind. The experimental apparatus which constitutes our aerosol generator is shown in Figure 4.5. A supersaturated solution of ammonium sulfate and water is placed in an airtight flask. Two tubes extend into the flask. One of these is open to the room and extends into the solution, acting as the intake. The exhaust extends into the empty space above the solution and is connected to the chamber inlet. As air passes through the flask it bubbles the solution releasing ammonium sulfate solution droplets which are carried into the chamber by the airflow. Since the room air is not filtered, we also expect some room aerosol to be carried into the chamber also.

For these tests, the clear viewing wall is in place and using a high intensity lamp, we can observe droplets after they have grown to a suitable size, which is about 1μ in radius. Our observations show droplet growth is sufficient for viewing after about 5-7 cm into the

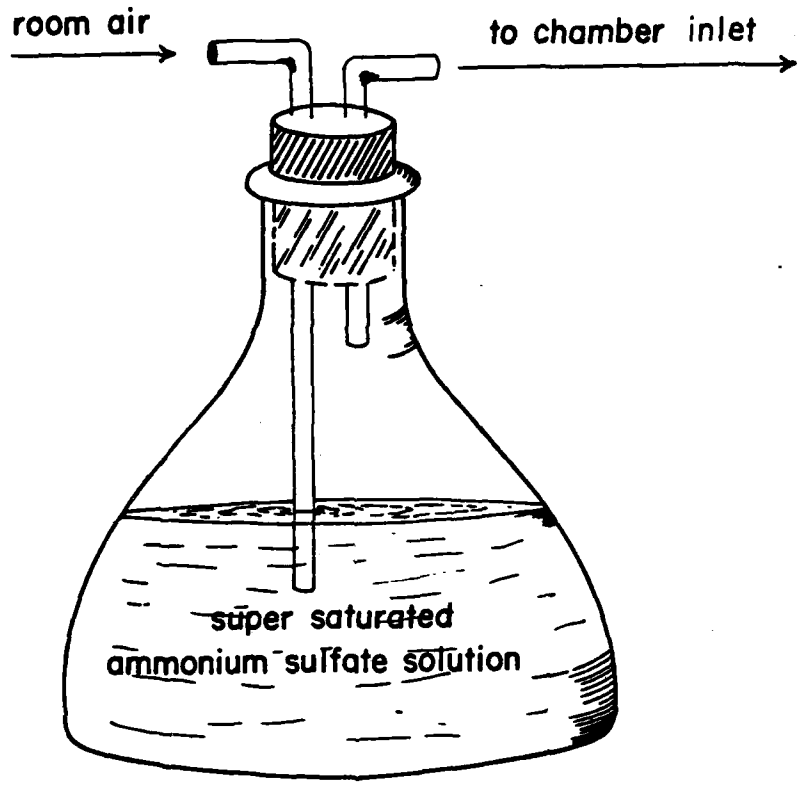

Figure 4.5 Aerosol Generator used to produce Ammonium Sulfate droplets.

chamber. The droplet concentration is much lower than the titanium tetra-chloride smoke so individual droplets could be followed to observe their travel through the chamber. Regardless of the flow rate, the flow is perfectly laminar and a droplet can be followed from first detection until it exits the chamber. Evidence of a constant humidity in the chamber is given by the fact that some droplets would travel half the distance of the chamber and since they were still growing would stop and begin to settle against the flow. It is this principle which we intend to use to suspend droplets for observation by counteracting this fall velocity.

Verifying that droplets are growing we now conducted tests of residence time in the chamber. The method used is similar to that of Hudson (1980) and Alofs (1978). The procedure follows. The chamber is operated at various flow rates according to the plug flow curve shown in Figure 4.3. The droplet size distribution is determined at each setting and plotted on a graph of concentration versus flow rate.

Providing that the chamber is operating properly, we expect the following results: first, the slower flow rates should show counts for only the smallest particles since the larger ones will settle out against the flow before reaching the optical counter. Since the CI-208 particle counter indicates the number of particles greater than the size being measured, then we expect a sharp increase in the concentration as the settling velocity for that size is exceeded. There should be a continued increase in concentration until the flow in the chamber produces a residence time the same as the growth time required for a

droplet to reach that equilibrium size. Since the rate of growth of droplets is rapid at first, we will also be counting droplets whose equilibrium size is greater than the size being counted. As the flow is further increased, then we expect a decrease in counts since fewer droplets are grown to the same size. The maximum therefore indicates that all droplets whose equilibrium radius is that size or less have grown to r_{100}. In this manner, the data gathered is the same as other isothermal haze chambers.

The measurements obtained in this manner are limited due to restrictions resulting from the particle detection system used. Our laboratory has two CI-208 particle detection systems. The newest system was purchased specifically for this project and is capable of measurements of droplets 10μ in size or larger. This range is vital for MOBIFOC since the droplets of most interest are 5μ or larger. Internal circuitry modification of this counter is necessary to perform these type of measurements, but scheduled changes were not completed in time to perform these tests. For this reason, we are using the same particle detection system used on the Fukuta and Saxena (1979a,b) Horizontal Thermal Gradient Cloud Condensation Nucleus Spectrometer which has had these modifications. This counter is an older model of the CI-208 and therefore cannot discriminate sizes greater than 3μ. Furthermore, calibration of the instrument below 4 particles per cubic centimeter is not possible. Since this concentration is higher than that to be expected from room aerosol with r_{100} equal to 3μ (Alofs, 1978) and our bubble burst generator produces an

insignificant number of salt particles with the same equilibrium size (Mason, 1954) we were limited to conducting our tests on droplet sizes of 2.5μ and smaller. Nevertheless, we have already demonstrated that velocity profiles, humidity, and laminar flow are present in our instrument at all flow rates, so there is no reason to doubt that if operation for smaller sizes is correct, then it will be accurate for larger sizes as well.

Figure 4.6 represents the results obtained from our experiments. As can be seen in the figure, the increase in number concentration begins at successively faster flow rates for increased droplet sizes. This is indicative that the flow is greater than the settling velocity. A plateau or maximum of droplet concentration is reached, but the decrease on the other side is not seen because of the limited flow rates of the flow meter used. The results indicate that our chamber is working satisfactorily.

We have previously mentioned that we have visually observed the ability to suspend particles in this chamber. In order to document this, we attempted to photograph suspended particles in the chamber. We were concerned that condensation on the side walls would obscure photographs, so we used large smoke particles of titanium tetrachloride. Photography was accomplished using a Canon 35 mm camera with macro lens. Kodak panatomic x film with an ASA of 32 was used. Illumination was provided with a high intensity microscope lamp and the shutter held open for 60 seconds. The method of suspension involved shaking smoke particles loose which had clung to the foam rubber of the exhaust cap and then adjusting the flow and belt until

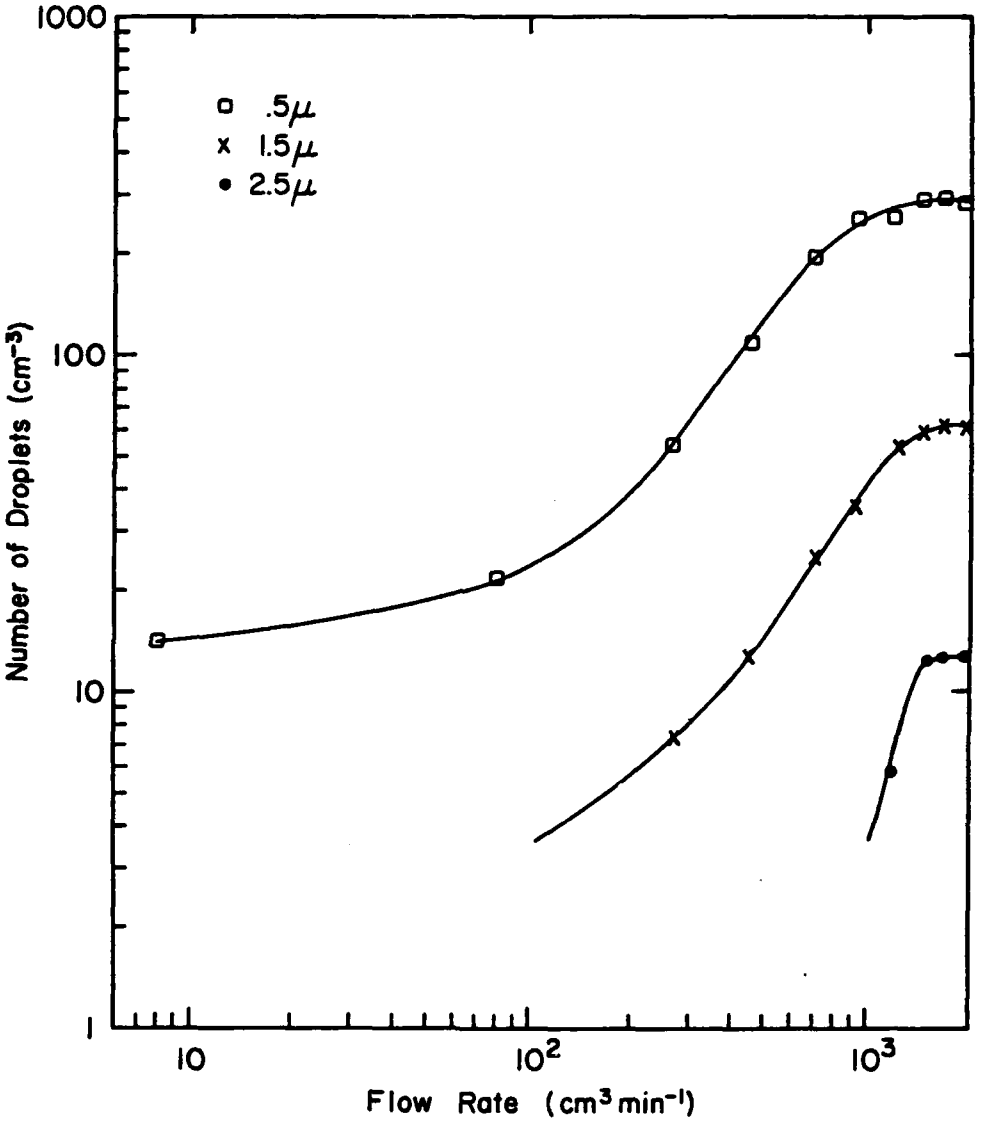

Figure 4.6 Cumulative size distribution vs. flow rate in chamber.

the particles were suspended within the camera's field of view. Figure 4.7 is the resulting photograph. The velocity at the time was close to 0.6 cmS^{-1} which corresponds to the fall velocity of a pure water droplet of about 23μ diameter. A group of three suspended particles are circled in the photograph.

Two other items of note can be seen in this photograph. The first is the laminar flow as indicated by the thin wispy streaks left by very small smoke particles remaining in the chamber from previous tests. Second, the streaks left by a larger particle which was settling against the flow can be seen as indicated by the arrow. We wondered why the streak was not parallel to the side walls of the chamber and found that the chamber had not been leveled before the photographs were taken. Particles moving with the flow or suspended do not appear to be affected by leveling, but we recommend that chamber be leveled before operation.

4.4 Further Observations

During the testing and evaluation procedures outlined, we continually observed droplet behavior in the chamber. Some interesting occurrences are worth noting. One of these is the variation of droplet size distribution and concentration under varied operating conditions. We noticed that at slow flow rates, a high number of small droplets were present in the chamber. Under these conditions, the droplets appeared to be relatively mono-disperse in size since all moved with nearly the same velocity. With higher flow rates, the droplet size distribution was obviously more varied with a lower concentration, but

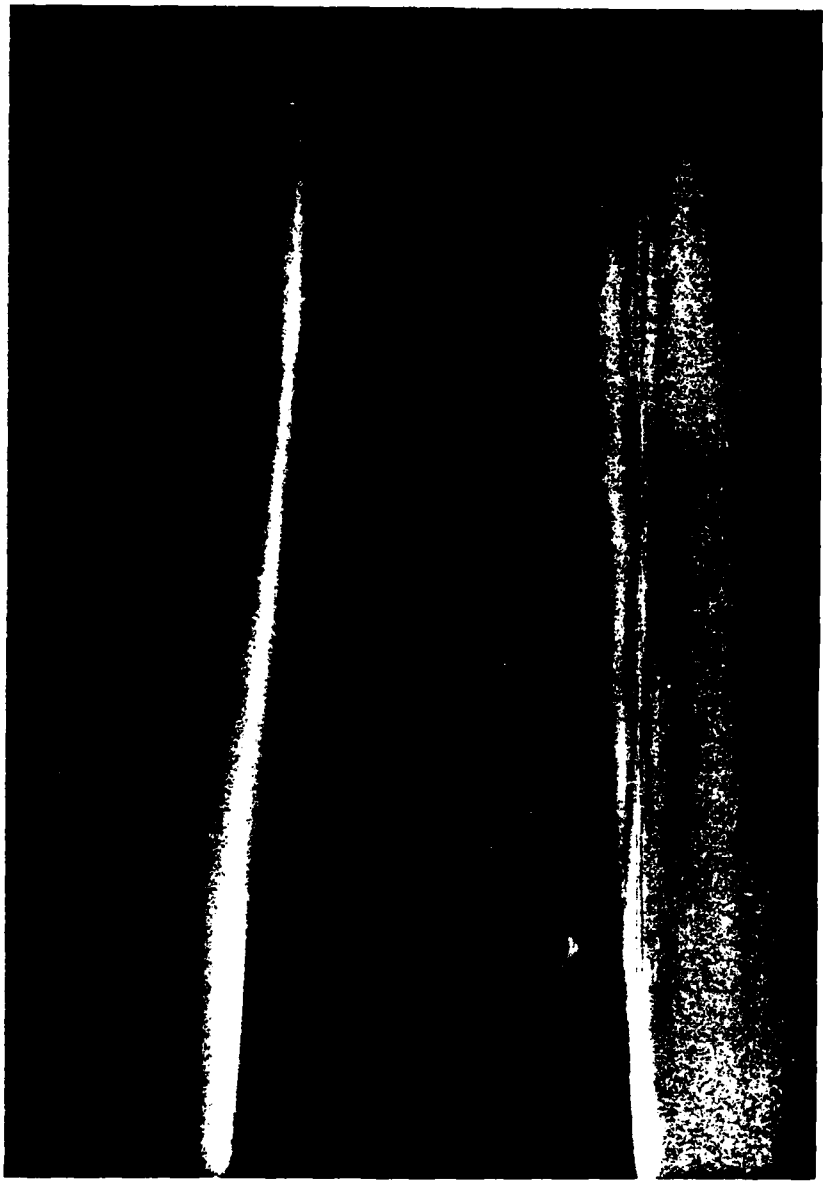

Figure 4.7 Time lapse photography of droplet suspension.

larger droplets. This was evidenced by the fact that there was a distinct difference in velocity of droplets and also that some would settle out against the flow. We attribute this disparity at different flows to our method of aerosol generation. At slower flow rates, much smaller bubbles were produced than at larger flow rates. The size of the bubble when it bursts has an affect on the size of the aerosol particle produced (Pruppacher and Klett, 1980) with larger bubbles generally producing larger salt particles.

During our test, we accidentally spilled water into the diffuser while filling the reservoir. This produced bubbles as air entered the diffuser. We were interested in observing differences when a different salt was used, so we used ordinary table salt and water in the diffuser inlet to produce the bubbles. Using this method, the droplets and aerosols were injected directly into the chamber. At slow flow rates there was no loss of salt nuclei and the resulting droplet formation was a highly concentrated haze of extremely small droplets. The droplet size is not much of a surprise since sodium chloride will produce smaller droplets than ammonium sulfate. The concentration was a surprise though since the haze was dense enough to reduce the visibility in the chamber. Again, these small droplets seemed to be mono-disperse with no noticeable size difference. We were also interested in the behavior at high flow rates, so we replaced the flow meter previously used with one that allowed much faster rates of flow. The flow was nearly doubled over that thus far used and vigorous bubble bursting occurred in the diffuser. The droplets produced in the

chamber were much larger than any previously seen. They were large enough that the sphericity of the droplets was easily noticed. We had no way of actually measuring the droplets at the time, but estimate the size to be between 10 and 50μ in diameter. This would be consistent with the flow speed in the chamber at the time since nearly half the droplets were carried through the chamber and removed while others apparently were still in a stage of rapid growth since they could be seen to stop and then begin to settle out rapidly to the bottom of the chamber.

Judging by these observations, it seems it may be possible to simulate rain in the chamber by producing a collision-coalescence process. We have shown the ability to suspend droplets and to produce a very large range of sizes and concentrations. If these conditions can be combined and controlled then the rain initiation process should be producible.

CHAPTER 5

5. DATA REDUCTION AND ERROR ANALYSIS

The instrument presented here has been shown through our operational tests to be well constructed and capable of the operational requirements set forth in the initial design phases. Errors in data obtained with the instrument will fall into two areas which we will discuss here. The first are errors due to the operational limitations and design of the instrument which cause inaccurate droplet size distributions. The second area of possible errors is in the method of analyzing the droplet size distributions obtained.

5.1 Errors Attributable to Instrument

5.1.1 Leaks. The most significant source of error with MOBIFOC results from the presence of leaks into the chamber. Leaks of outside air into the chamber prevent the sample air from being drawn into the diffuser inlet thereby reducing the number concentrations measured. It is easy to determine if leaks are present and we have already outlined the method in a previous chapter. It is repeated here since this is extremely important if accurate results are to be obtained. At high flow rates, most leaks will not be noticeable since the main flow is so large that it overwhelms the minor leaks. It is also reasonable to assume that any errors due to leaks at large flow rates will be small and quite possibly neglible. At low flow rates, however, the presence of small leaks in the chamber become so important that they may entirely prevent sample introduction into the diffuser inlet. Our method of insuring that chamber is leak free is to place the sample

inlet tube in a beaker of water. If water is drawn into the tube at the slowest flow rates then leaks are sealed and measurements are guaranteed accurate.

We have been unable to devise a foolproof method of locating all leaks and therefore suggest that after all adjustments of belt tensions have been completed and locked and other preparations of the chamber completed for operation, a bead of sealant be placed over each connecting piece of the instrument including the screw holes. If care is taken this will eliminate all leaks.

5.1.2 Residence Time. In our calibration tests of residence time we verified growth times by establishing a maximum of number concentrations corresponding to the growth time and size of droplets. We mentioned that the maximum shows a higher count than the actual number of droplets which have attained their equilibrium size. This is not a problem unique to MOBIFOC, but it is present in all the isothermal haze chambers currently in use. The problem has not been addressed in the literature, most likely because there is no guaranteed method of determining the magnitude of error. We expect that MOBIFOC would have a lower error rate in this respect since when larger particles begin to settle, they settle against the flow and will not be counted, whereas in previous instruments, they will fall directly into the droplet counter.

The amount of error should be most significant at small droplet sizes since these tend to act as gases being advected with the flow and not settling out. At larger sizes, (>2μ) the error is reduced

partly because droplets will settle out before reaching the counter and partly due to the typical size concentrations of large droplets which are very low. In an uncontrolled environment such as field testing, the problem is increased since the droplets formed in the chamber will have different densities and shapes, and settling velocities will vary greatly for a given size (Friedlander, 1977). Hudson (1980) experienced this difficulty in field calibration tests especially with droplets less than 3μ in size as we predicted. He suggests that the cause was droplet evaporation in the optical detection system, but this problem was not encountered during controlled laboratory tests. We disagree with his conclusions attributing the majority of discrepancies to the variation in natural aerosols.

5.2 Droplet Growth Time

The ability of an instrument such as MOBIFOC to perform the task of deriving activation spectra is based solely on droplet growth theory. Thermal and Chemical Gradient diffusion cloud chambers also rely heavily on this same theory but with one major difference. The latter grow droplets in a regime of unstable growth while isothermal haze chambers grow droplets in the stable equilibrium regime.

Droplet growth time at 100% relative humidity has received little attention in the literature. Laktionov (1972) utilized the results of Aleksandrov et al. (1969) in determining the growth time for droplets in his isothermal haze chamber. Because Aleksandrov et al. (1969) is available at only one or two locations in this country and only in Russian, other researchers have relied on Laktionov's

interpretation of their data. We have been fortunate enough to obtain the original publication and to have it translated in order to verify Laktionov's conclusions. Figure 5.1 shows a graphical representation of the tables generated by Aleksandrov et al. This particular figure represents growth of water droplets on sodium chloride nuclei at 100% relative humidity and 20°C at sea level, for both 100% and 1% soluble nuclei. Because the growth curves approach r_{100} exponentially in time, previous researchers have chosen the time it takes to reach $.95\, r_{100}$ as the growth time in their chambers. From the curves presented in Figure 5.1, we have located $.95\, r_{100}$ and determined the best line fit to the points. For reference, we have indicated the line representing the growth time of Laktionov.

Until recently, the values of Aleksandrov et al. were the only growth times available. Robinson and Scott (1981) presented a new growth rate formula (NGRF) which produced substantially different growth times. Plotted on Figure 5.1 is also the growth times of Robinson and Scott.

We are not in a position to determine which of the growth times is most accurate. We prefer to use those determined by us from interpolation of the data, not in vanity, but since they are the longest of the sets of times and therefore a more conservative value. If our growth times are longer than that actually required, no error results since droplets cannot grow beyond their equilibrium size. An interesting feature to note is that basically the same time is required to reach $.95\, r_{100}$ regardless of the solubility of the nucleus.

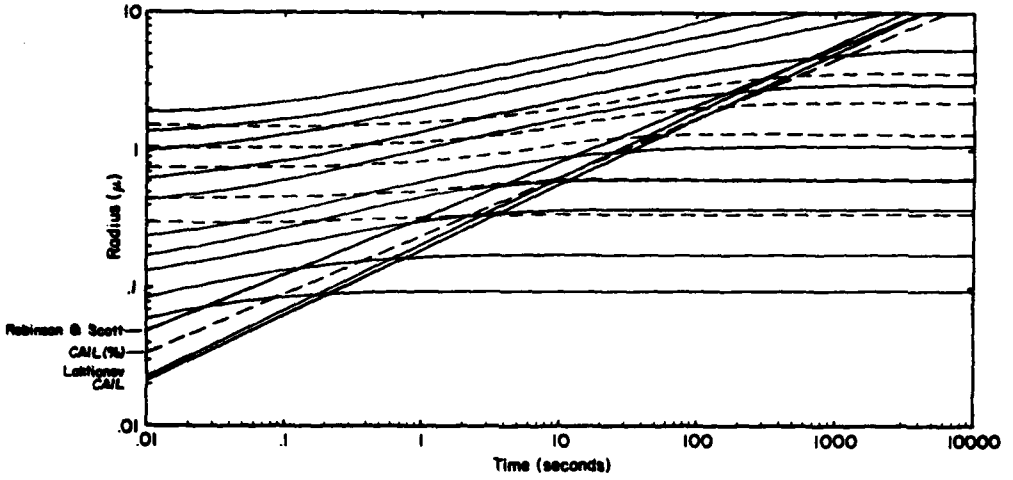

Figure 5.1 Droplet growth at 100% relative humidity. Straight lines represent growth time to .95 r_{100}.

This is advantageous since we can now be assured that all drops of a given size in our chamber have been fully grown. This convenience has not been noted by other researchers who have generally ignored the presence of less soluble nuclei.

5.3 Approximation Formulas

A large fraction of hygroscopic nuclei that participate in the formation of fog and haze in the lower troposphere consists of sulfate particles (Hänel, 1981b; Rahn and McCaffrey, 1981). That these sulfate aerosols play a dominating role in the global sulfur budget is well documented (Friend, 1973; Altshuller, 1973). Growth of particles from the dry state to haze and fog droplets depends upon their initial radius, density and surface tension of the solution droplet, and concentration of the solute in droplets. That these factors are much more crucial for the sulfate aerosols than, for example, sodium chloride is a result of the solubility of the sulfate in water. It will be demonstrated in this section that sulfates are generally the least soluble of all the nineteen electrolytes which have been extensively studied (Low, 1969) and that sulfate droplets between 80% relative humidity and the critical supersaturation cannot be regarded to consist of weak solutions - an assumption commonly used in the literature (Pruppacher and Klett, 1980; Chýlek and Ramaswamy, 1982) and in the study of fog and haze droplets in isothermal haze chambers (Laktionov, 1972; Fitzgerald, 1975).

5.3.1 Classification of Electrolytes. An electrolyte when dissolved in water has the ability to alter the physical characteristics of the resulting solution as compared to pure water. Surface tension and density of the solution droplets vary with the solution concentration and the droplet diameter approaching the values for pure water at weak concentrations and large diameters. These variables are affected in varying degrees by the electrolytes characteristics including the crystalline structure of the salt, ionic charge and size of molecules, lattice energy of salt crystals, and surfactants present in the solution droplets. Relative importance of these factors vary with the electrolytes and render solution droplet growth behavior quantitatively unpredictable.

The Köhler equation which relates the saturation ratio S to the radius, r, of the solution droplet, may be written (e.g., Pruppacher and Klett, 1980) as

$$S = (1-b)\ \exp(\alpha/r) \tag{5.1}$$

or

$$S = 1 + \alpha/r - \beta/(r^3 - r_i^3) \tag{5.2}$$

where

$$\alpha = 2\sigma'/(\rho_w R_v T)$$

and

$$\beta = 3iM_w m_s/(4\pi\rho_w M_s)$$

and

$$b = iM_w m_s/m_w M_s$$

where T is the absolute temperature of the droplet, σ' the surface tension of the solution droplet, ρ_w the density of water, R_v the gas constant for water vapor; M_w and M_s, and m_w and m_s are the molecular weights and masses of the water and solute respectively; and i is the van't Hoff factor which depends upon the solution concentration and represents the degree of ionic dissociation. Radii of the solution droplet and of the insoluble material inside the droplet are denoted by r and r_i respectively. Solution concentrations are represented in molalities as defined as

$$\mu = 1000\ \xi_s/(M_w\xi_w) \tag{5.3}$$

where ξ_s and ξ_w respectively represent the number of moles of solute and water.

Let us define a weak solution as the one in which the values of the van't Hoff factor, solution density, and solution surface tension deviate 1% or less from their values for pure water. In Table 5.1 nineteen electrolytes which are of interest in cloud and aerosol physics (Low, 1969) have been classified into three classes depending upon the concentrations at which they may be considered as weak solutions. It is readily apparent that all the sulfates are Group III electrolytes which are the least soluble. It should also be noted that the chlorides may be considered weak solutions at concentrations three times as high as sulfates. Since most continental aerosol have been found to contain sulfates, (Hänel, 1981b) this is the main reason why the weak solution assumption is invalid for haze and fog droplets. This has been pointed out by some authors (e.g., see Hänel, 1976) but the resulting errors have not been analyzed. Estimation of errors are

Table 5.1. Classification of electrolytes. Classification according to the maximum concentrations at which they become weak aqueous solutions. Electrolytes are listed in descending order of solubility in water.

ELECTROLYTE	WEAK CONCENTRATION (Molality)	CRYSTAL STRUCTURE	IONIC CHARGE (of + and -ion)	LATTICE ENERGY ($KJ\ mol^{-1}$)
GROUP I				
LiCL	.015	cubic	1/1	834
NaBr	.015	cubic	1/1	732
NH_4NO_3	.015	rhombic	1/1	661
$NaNO_3$	.015	rhombic	1/1	755
NaCl	.015	cubic	1/1	769
NH_4Cl	.015	cubic	1/1	n/a
KBr	.015	cubic	1/1	671
KI	.015	cubic	1/1	632
KCl	.015	cubic	1/1	701
GROUP II				
$CaCl_2$	.010	cubic	2/1	2223
$MgCl_2$	.010	hexagonal	2/1	2326
$Zn(NO_3)_2$	.010	tetragonal	2/1	2376
$BaCl_2$	.010	cubic	2/1	2033
KNO_3	.010	rhombic	1/1	685
GROUP III				
$(NH_4)_2SO_4$	.005	rhombic	1/2	1766
Na_2SO_4	.005	rhombic	1/2	1827
$ZnSO_4$	.005	rhombic	2/2	3100
$MgSO_4$	.005	rhombic	2/2	n/a
$CuSO_4$	.005	rhombic	2/2	2276

AD-A119 730 AIR FORCE INST OF TECH WRIGHT-PATTERSON AFB OH F/G 4/2
MOVING BOUNDARY ISOTHERMAL FOG CHAMBER (MOBIFOC).(U)
MAY 82 G F FISHER
UNCLASSIFIED AFIT/CI/NR/82-52T NL

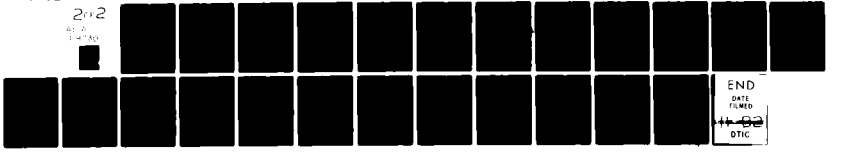

presented in the following sections for NaCl and $(NH_4)_2SO_4$. These electrolytes are used since they are representative of their groups and are most commonly found in marine and continental aerosols.

5.3.2 Theoretical Considerations. One of the consequences of the preceeding is that in a humid environment, sulfate particles will have different equilibrium and critical radii than the chloride or nitrate aerosols. The critical supersaturation $S_c(\%)$, may be obtained from the maximizing condition for the Köhler curve represented by (5.2) and assuming a weak solution:

$$S_c(\%) = 38.5\ \alpha(\alpha/\beta)^{\frac{1}{2}}. \tag{5.4}$$

In a water saturated environment which is prone to fog and haze formation, S=1 and (5.2) yields

$$r_{100} = (\beta/\alpha)^{\frac{1}{2}}. \tag{5.5}$$

However, the critical radius of a hygroscopic nucleus corresponding to S_c in (5.4) becomes

$$r_c = (3\beta/\alpha)^{\frac{1}{2}} \tag{5.6}$$

Haze and fog droplets which form on hygroscopic aerosols and grow to r_{100} at 100% relative humidity, acquire r_c if subjected to a supersaturated environment of $S = S_c$. From (5.4) and (5.5), S_c for a hygroscopic nucleus which undergoes unstable growth, may be expressed in terms of r_{100},

$$S_c(\%) = 38.5\alpha/r_{100}. \tag{5.7}$$

If r_o is the radius of a dry aerosol particle, S_c may be related (Fitzgerald, 1975; Fitzgerald, 1974) to r_o as

$$S_c(\%) = kr_o^{-3/2} \tag{5.8}$$

where k varies with the electrolyte but may approximately be assigned (Fitzgerald and Hoppel, 1981) an average value of 1.7×10^{-3} for ammonium sulfate and 1.2×10^{-3} for sodium chloride based on recent measurements. Assuming the aerosol particles are spherical, their dry radius is determined from their mass as

$$r_o = (3m_s/4\pi\rho_s)^{1/3} \tag{5.9}$$

where ρ_s is the density of the electrolyte.

Equation (5.7) was first introduced by Laktionov (1972) in the determination of the activation spectra of aerosols responsible for producing haze and fog and was subsequently used for determination of S_c with the help of isothermal haze chambers (Hudson, 1980, Alofs, 1978). Since α depends upon the properties of the water substance, at T = 293K, the following numerical values in c.g.s. units may be assigned to the coefficients in (5.5) - (5.7);

$$r_{100} = .0414 S_c^{-1} \tag{5.10}$$

$$r_c = .0717 S_c^{-1} \tag{5.11}$$

$$r_c = \sqrt{3} r_{100} \tag{5.12}$$

again, assuming that droplets exist in a weak solution and r_{100} and r_c are in microns, and S_c in percent. (5.10) - (5.12) have been used extensively in the study of haze formation and considered as unique relationships (Hudson, 1980; Hoppel and Fitzgerald, 1977; Hoppel, 1979). In reality, these relationships are far from being unique as is obvious from the preceeding discussion of the classification of electrolytes.

5.3.3 Activation Spectrum of Sulfate Aerosols. The preceeding equations and formulas have been used extensively in isothermal haze chambers to determine the activation spectra of solution droplets. Since sulfate aerosols cannot be considered a priori weak solution droplets, appreciable errors result in these estimations.

In order to determine the magnitude of errors involved, values of S were determined for various radii at given masses of $(NH_4)_2SO_4$ and NaCl using (5.1). This form of the Köhler equation was used since it was determined that truncated exponential expansion led to appreciable errors at the smallest radii. Computations were accomplished on the CAIL's TRS-80 microcomputer system. The algorithm used in computation selected a radius, and the solution concentration determined as

$$\text{concentration} = 3m_s/\{4\pi(r^3-r_i3)\}. \tag{5.13}$$

If ε is the fraction of nucleus which is soluble defined as

$$\varepsilon \equiv m_s/(m_s + m_i) \tag{5.14}$$

where m_i is the mass of insoluble material, then we use the definition of density and the formula for volume to find r_i thusly:

$$r_i = \{3(m_s/\varepsilon-m_s)/4\pi\rho_i\}^{1/3}. \tag{5.15}$$

In our calculations, we used quartz (SiO_2) as the insoluble material with a density of $\rho_i = 2.65 gcm^{-3}$. Using data for aqueous solutions presented in the CRC Handbook of Chemistry and Physics and by Low (1969) the values of α, β and b in (5.1) and (5.2) were computed through interpolation, and a value of S determined for each equation. To determine r_{100} and r_c, we first determined the interval of radii in which each occurred, and then through subsequent halving of the

interval determined the radius where S=100% relative humidity, and where S was maximized. In this manner there is no error in r_{100}, and less than 0.5% error in S_c. The error in r_c is considerably more. We estimate the error in the critical radius to be as high as 6% in a few cases and less than 2% in the majority of cases. The values were calculated for sodium chloride and ammonium sulfate with masses of 10^{-18} to 10^{-12} grams and for ε =1,.1 and .01. Greater accuracy in r_c is possible by lengthening the numerical scheme used. However, the calculations required over 70 hours of time on the TRS-80 and we felt that extra time did not justify greater precision. Table 5.2 summarizes our results showing the equilibrium droplet size at 100% relative humidity and the solution concentration of the droplet at that point.

In isothermal haze chambers, the method to determine the activation spectra is to measure r_{100} and then to derive the other parameters using (5.9) - (5.11). To determine the amount of error arising from the use of these approximation formulas, we used our calculated values for real solution concentrations to determine the value of the "constant" in each of equations (5.10) - (5.12) and (5.8). To determine the percent error arising, the following formulas are used:

$$\eta_1 = \left(1 - \frac{r_o^{3/2} S_c}{k}\right) x100 \qquad (5.16)$$

$$\eta_2 = \left(1 - \frac{r_{100} \cdot S_c}{.0414}\right) x100 \qquad (5.17)$$

Table 5.2 Solution concentrations of droplets. Concentration of solution in droplets at the equilibrium radius, r_{100}.

ELECTROLYTE	% SOLUBLE	MASS OF SOLUTE (grams)	r100 (μ)	MOLALITY
SODIUM CHLORIDE	100%	10^{-18}	0.012	2.352
		10^{-17}	0.036	0.880
		10^{-16}	0.113	0.288
		10^{-15}	0.359	0.089
		10^{-14}	1.159	0.026
		10^{-13}	3.688	0.008*
		10^{-12}	11.680	0.003*
	10%	10^{-18}	0.014	2.069
		10^{-17}	0.039	0.821
		10^{-16}	0.116	0.280
		10^{-15}	0.362	0.088
		10^{-14}	1.162	0.026
		10^{-13}	3.691	0.008*
		10^{-12}	11.682	0.003*
	1%	10^{-18}	0.023	1.353
		10^{-17}	0.054	0.596
		10^{-16}	0.138	0.234
		10^{-15}	0.390	0.082
		10^{-14}	1.191	0.026
		10^{-13}	3.720	0.008*
		10^{-12}	11.717	0.003*

(Continued)

Table 5.2 Solution concentrations of droplets. Concentration of solution in droplets at the equilibrium radius, r_{100}. (Continued)

ELECTROLYTE	% SOLUBLE	MASS OF SOLUTE (grams)	r100 (μ)	MOLALITY
AMMONIUM SULFATE	100%	10^{-18}	0.009	3.419
		10^{-17}	0.025	1.266
		10^{-16}	0.080	0.355
		10^{-15}	0.266	0.097
		10^{-14}	0.928	0.023
		10^{-13}	2.989	0.007
		10^{-12}	9.502	0.002*
	10%	10^{-18}	0.012	2.643
		10^{-17}	0.030	1.046
		10^{-16}	0.086	0.329
		10^{-15}	0.272	0.094
		10^{-14}	0.932	0.023
		10^{-13}	2.993	0.007
		10^{-12}	9.505	0.002*
	1%	10^{-18}	0.022	1.455
		10^{-17}	0.049	0.606
		10^{-16}	0.119	0.232
		10^{-15}	0.321	0.076
		10^{-14}	0.977	0.022
		10^{-13}	3.038	0.007
		10^{-12}	9.551	0.002*

*INDICATES WEAK SOLUTION

$$n_3 = \left(1 - \frac{r_c \cdot S_c}{.0717}\right) x100 \qquad (5.18)$$

$$n_4 = \left(1 - \frac{r_c}{\sqrt{3}\, r_{100}}\right) x100 \qquad (5.19)$$

Where $n_{1,2,3,4}$ refer to the % error arising from the use of equations (5.8) and (5.10)-(5.12) respectively. The results of our calculations are shown in Figure 5.2. The figures are presented in a way that shows not only the error to be expected, but also demonstrates the deviation from straight line relationships assumed with the weak solution. Indicated in each figure is the mass at which the solution droplet may be considered weak by our definition and classification scheme given in Table 5.1. Since we are primarily concerned with the analysis of data from isothermal haze chambers, we have also boxed in the portion of figures which is of concern in these instruments, namely those droplets whose critical supersaturation lies between 0.1 and 0.01%. The activation spectra obtained from isothermal haze chambers exclusively depends on (5.10) while other parameters may be derived from the other relationships. As we can see from the figures, appreciable errors arise from the use of the approximation equations, especially under stronger solutions. The largest errors are with Ammonium Sulfate in particular or the less soluble Class III electrolytes in general. However, if we restrict our use of the approximation formulas to the supersaturation range less than 0.1%, as in an isothermal haze chamber, the resulting errors should be less than 5% in derived critical supersaturations and approaching 10% for the critical radius. Therefore, we conclude

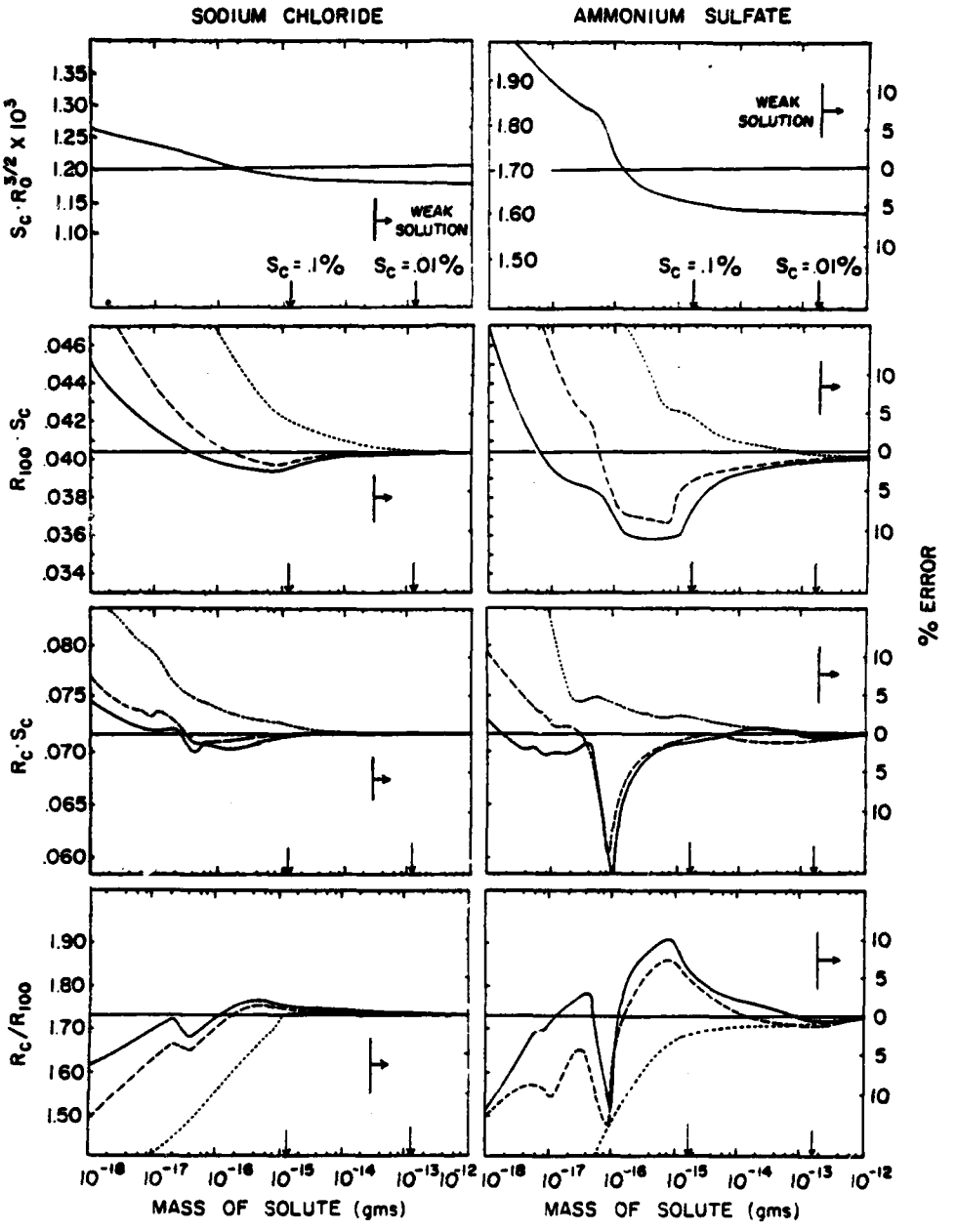

Figure 5.2 Errors resulting from use of approximation formulas. Solid lines represent 100% soluble nucleus, dashed 10%, and dotted lines, 1% soluble nucleus.

that the errors present in the approximation formulas (5.10)-(5.12) will yield acceptable results in determination of the activation spectrum. Use of equation (5.8) should be forbidden. Errors are less than 5% in only a very narrow range and only for 100% soluble nuclei. For ε=.1 and .01 the errors are greater than 250% and 600% respectively.

The results presented here indicate that use of formula (5.10) to determine S_c will yield a higher S_c than that actually attributable to the solution droplet. This occurs however only for the smaller droplets with S_c near 0.1%. The error is 5% decreasing to nearly zero for droplets with S_c near .01%. If we refer once again to the growth times presented earlier in Figure 5.1, we see that the smaller drops are full grown to r_{100} in the chamber while the larger are only grown to $.95r_{100}$. The effect of growing to $.95r_{100}$ is to also increase the derived supersaturation by 5%. So we find that our error is nearly constant throughout the normal operation of the chamber. By simply reducing all our results by 5%, we can nearly eliminate any error entirely. Both Hudson (1980) and Alofs (1978) have indicated a gap between measurements obtained from Thermal Diffusion Chambers and their isothermal haze chambers in the region where the two instruments overlap. We took their data and reduced the supersaturations they derived through use of these approximation formulas by 5% and found that this eliminated most gaps in the measurements showing nearly perfect agreement between the two instruments as should be. Our results are shown in Figure 5.3.

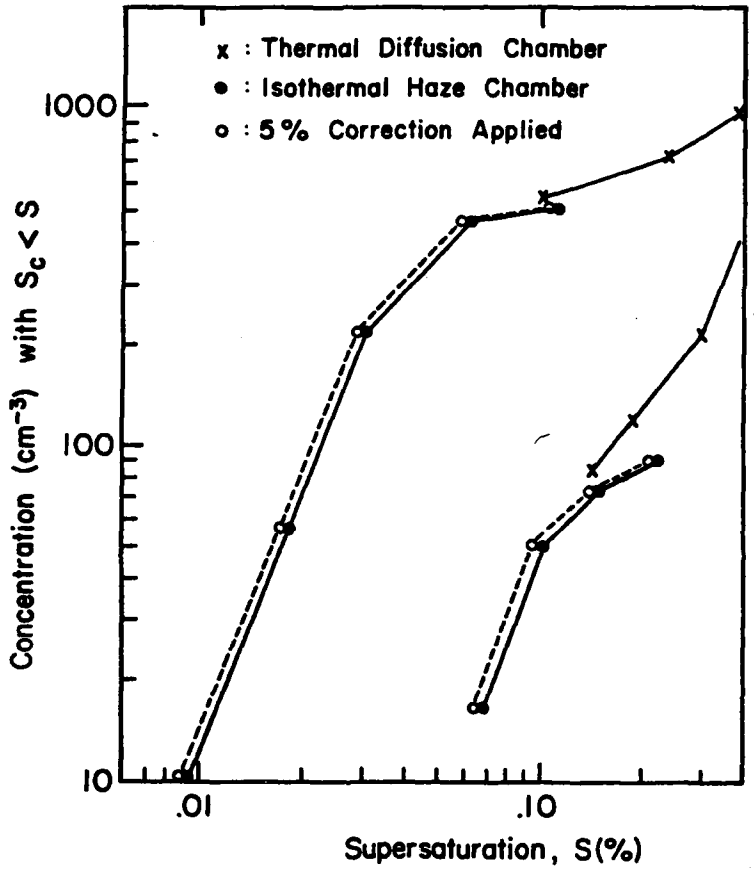

Figure 5.3 An application of correction to approximation formulas.

CHAPTER 6

6. SUMMARY AND CONCLUSIONS

In the attempt to develop a new instrument which will extend our current knowledge of supersaturation spectra, a number of innovations have been introduced. Significant contributions to cloud physics instrumentation have been achieved as well as a versatility not presently available in one instrument. The main contributions are listed below.

6.1 Instrument Development

The possibility of a continuous flow, isothermal fog chamber with greatly extended growth times was expressed by Saxena (1980 - personal communication). The development of MOBIFOC demonstrates the concept. The innovative and unique features of the instrument are:

1. Moving boundaries within an isothermal chamber have been constructed and successfully tested. The establishment of plug flow in the chamber has been shown to exist as well as other velocity profiles as desired.
2. An automatic continuous moisture supply has been employed which is entirely self contained.
3. Direct observation of the interaction of droplets with water vapor and other droplets is provided.
4. The ability to suspend droplets over a wide range of sizes and long periods of time has been demonstrated. This allows for prolonged studies of dynamic changes and interactions which may occur in the vicinity of a droplet.

Other major contributions include the production of an isothermal haze chamber which is lightweight and portable for use in aircraft and field experimentation. The design is simple to construct and operate and provides for ease of access for maintenance.

6.2 Other Findings

In addition to the development and introduction of a new instrument, extensive study has been conducted in the area of droplet formation and growth as pertains to the analysis of data. The main results of this study are:

1. Nineteen common electrolytes have been classified into three classes according not only to their solubility, but also to the solution concentrations at which they may be treated as weak solutions.
2. Approximation formulas commonly used in the literature to derive critical parameters of droplets have been shown to contain large errors. However, in the region of operation of isothermal haze chambers, these errors are shown to be generally less than 5%.
3. A method to eliminate errors caused by use of the approximation formulas is introduced. Two examples of the method are presented to show the result.

6.3 Possible Future Applications of MOBIFOC

The unique features of MOBIFOC, namely adjustable plug flow and moving boundaries, suggest a wide range of applications beyond use as an isothermal fog chamber.

1. MOBIFOC may be used as a standard against which other isothermal haze chambers may be calibrated.
2. Testing and verification of droplet growth times on various aerosols composed of different nuclei can be conducted.
3. Separate reservoirs allow for different solutions to be used on either side of chamber creating relative humidity gradients. Droplet growth under relative humidities less than 100% is also possible.
4. Studies of chemical transformation processes, growth passivation or haze modification are possible by introducing interactive materials with suspended droplets in the chamber.
5. Visibility studies in haze and fog may be conducted through use of the clear observation wall.
6. The ability to suspend droplets may be extended to ice crystals where growth, settling, and splintering mechanisms may be studied in simulated natural environment.
7. Heating elements may be easily installed allowing MOBIFOC to act as a Thermal Gradient Diffusion Cloud Chamber. The versatility of velocity profiles can be utilized to counteract phoretic forces allowing for operation at very low supersaturations and prolonged growth times.
8. Experiments to determine condensation coefficients may be conducted with greater precision than presently allowed and over a wider range of aerosols and saturation ratios.

7. LIST OF REFERENCES

Aleksandrov, E. L., L. M. Levin and Yu. S. Sedunov. 1969. Condensation Growth of Drops on Hygroscopic Nuclei. Tr. IEM No. 6, 16-96.

Alofs, D. J. 1978. Performance of a Dual-Range Cloud Nucleus Counter. J. Appl. Meteor. 17:1286-1297.

Alofs, D. J. and J. C. Carstens. 1976. Numerically Simulated Performance of Widely Used Cloud Nucleus Counter. J. Appl. Meteor. 15:350-354.

Alofs, D. J. and T. Liu. 1981. Atmospheric Measurements of CCN in the Supersaturation Range 0.013-0.681%. J. Atmos. Sci. 38:2772-2778.

Altshuller, A. P. 1973. Atmospheric Sulfur Dioxide and Sulfate: Distribution of Concentration at Urban and Nonurban Sites in United States. Environ. Sci. Tech., 7:709-712.

Amelin, A. G. 1967. "Theory of Fog Condensation." Israel Program for Scientific Translations, Ltd., 236 pp.

Berg, T. G. O. and D. C. George. 1968. Investigation of the Kinetics of Condensation. J. Geophys. Res. 73:3103-3112.

Bird, R. B., W. E. Stewart and E. N. Lightfoot. 1960. Transport Phenomena." John Wiley & Sons. 780 pp.

Bradley, S. G. 1981. The Relation Between Cumulus Albedo and Extinction Coefficient and its Application to Remote Sensing. J. Atmos. Sci. 38:2243-2256.

Braham, Jr., R. R. 1974. Cloud Physics of Urban Weather Modification. A Preliminary Report. Bull. Amer. Meteor. Soc., 55:100-106.

Byers, H. R. 1974. "General Meteorology." McGraw-Hill, 461 pp.

Changnon, S. A. 1981. Midwestern Cloud, Sunshine and Temperature Trends since 1901: Possible Evidence of Jet Contrail Effects. J. Appl. Meteor. 20:496-508.

Changnon, Jr., S. A., R. R. Braham et al. 1975. The Role of Aerosols in Producing Inadvertent Weather and Climate Modification. Chemist. Meteor. Workshop, 1975. 13-17 January 1975, Ft. Lauderdale, FL., D. H. Slade, Ed., 40-44.

Chýlek, P. and V. Ramaswamy. 1982. Simple Approximation for Infrared Emissivity of Water Clouds. J. Atmos. Sci. 38:171-177.

DeSalmand, F. and R. Serpolay. 1982. Comparison of Parallel Plate Thermal Diffusion Chambers used for Measuring the Cloud Condensation Nuclei Concentration in the Atmosphere. J. Atmos. Sci. 39:000-000.

Detwiler, A. G. and B. Vonnegut. 1981. Humidity Required for Ice Nucleation from the Vapor onto Silver Iodide and Lead Iodide Aerosols over the Temperature Range -6^{o} to -67^{o}C. J. Appl. Meteor. 20:1006-1012.

Fitzgerald, J. W. 1974. Effect of Aerosol Composition on Cloud Droplet Size Distribution: A Numerical Study. J. Atmos. Sci. 31:1358-1367.

Fitzgerald, J. W. 1975. Approximation Formulas for the Equilibrium Size of an Aerosol Particle as a Function of its Dry Size and Composition and the Ambient Relative Humidity. J. Appl. Meteor. 14:1044-1049.

Fitzgerald, J. W. 1978. A Numerical Model of the Formation of Droplet Spectra in Advection Fogs at Sea and its Applicability to Fogs off Nova Scotia. J. Atmos. Sci. 1522-1535.

Fitzgerald, J. W. and W. A. Hoppel. 1981. Measurements of the Relationship Between the Dry Size and Critical Supersaturation of Natural Aerosol Particles. Present at IAMAP Conf. on Condensation and Ice Nuclei, Hamburg, Germany, August 1981.

Fitzgerald, J. W., C. F. Rogers and J. G. Hudson. 1981. Review of Isothermal Haze Chamber Performance. Third Intl. Cloud Condensation Nuclei Workshop, Reno, Nevada, 6-17 October 1980, NASA Conf. Pub. 2212, 85-92.

Friedlander, S. K. 1977. "Smoke, Dust and Haze." Wiley, 317 pp.

Friend, J. P. 1973. The Global Sulfur Cycle. "Chemistry of the Lower Atmospnere." S. I. Rasool, Ed. Plenum Press. 177 pp.

Fuchs, N. A. 1959. "Evaporation and Droplet Growth in Gaseous Media." Pergamon Press. 72 pp.

Fukuta, N. and V. K. Saxena. 1979a. A Horizontal Thermal Gradient Cloud Condensation Nucleus Spectrometer. J. Appl. Meteor. 18:1352-1362.

Fukuta, N. and V. K. Saxena. 1979b. The Principle of a New Horizontal Thermal Gradient Cloud Condensation Nucleus Spectrometer. J. Rech. Atmos. 13:169-188.

Grant, L. O. 1971. Introduction. Second International Workshop on Condensation and Ice Nuclei, 5-19 August 1970, Ft. Collins, Co., compiled by L. O. Grant, 1.

Hänel, G. 1976. The Properties of Atmospheric Particles as a Function of Relative Humidity at Thermodynamic Equilibrium with the Surrounding Moist Air. "Advances in Geophysics." 19:73-188.

Hänel, G. 1981a. An Attempt to Interpret the Humidity Dependencies of the Aerosol Extinction and Scattering Coefficients. Atmos. Environ. 15:403-406.

Hänel, G. 1981b. Influences of Physical and Chemical Properties of Atmospheric Particles on the Activation Process in Fog Clouds. Beitr. Phys. Atmos. 54:159-172.

Hayashi, Y. and D. J. Golder. 1981. The Effects of Condensational Heating on Midlatitude Transient Waves in their Mature Stage: Control Experiments with a GFDL General Circulation Model. J. Atmos. Sci. 38:2532-2539.

Hindman, E. E. 1981. An Airborne Isothermal Haze Chamber. Third Intl. Cloud Condensation Nuclei Workshop, Reno, Nevada, 6-17 October 1980, NASA Conf. Pub. 2212, 28-32.

Hoppel, W. A. 1979. Measurement of the Size Distribution and CCN Supersaturation Spectrum of Submicron Aerosols over the Ocean. J. Atmos. Sci. 36:2006-2015.

Hoppel, W. A. 1981. Description of the NRL Isothermal Haze Chamber. Third Intl. Cloud Condensation Nuclei Workshop, Reno, Nevada, 6-17 October 1980, NASA Conf. Pub. 2212, 42-43.

Hoppel, W. A. and J. W. Fitzgerald. 1977. Measurement of CCN Spectra at Low Supersaturation in Relation to Fog Formation off the Coast of Nova Scotia. Proc. Symposium on Radiation in the Atmosphere, Science Press. 62-64.

Hudson, J. G. 1980. Relationship Between Fog Condensation Nuclei and Fog Microstructure. J. Atmos. Sci. 37:1854-1867.

Hudson, J. G. and P. Squires. 1976. An Improved Continuous Flow Diffusion Cloud Chamber. J. Appl. Meteor. 25:776-782.

Jayaweera, K. 1981. Personal Communication. Note: Research Proposal to NSF. Title: Arctic Stratus Cloud Experiment - Analysis of Cloud Physics and Meteorological Data.

Kassner, J. L. Jr., J. C. Carstens, M. A. Vietti, A. H. Bierman, P. C. P. Yue, L. B. Allen, M. R. Eastburn, D. D. Hoffman, H. A. Noble and D. L. Packwood. 1967. Expansion Cloud Chamber Technique for Absolute Aitken Nuclei Counting. IAMAP International Atmospheric Nuclei Instrument Workshop, Lannemezan, France, 8-23 September 1967.

Kocmond, W. C., C. F. Rogers and S. W. Rea. 1981. Introduction. Third International Cloud Condensation Nuclei Workshop, 6-17 October 1980, Reno, Nevada. NASA Conf. Pub. 2212, 1.

Köhler, H. 1936. The Nucleus in and the Growth of Hygroscopic Droplets. Trans. Faraday Soc. 32:1152.

Laktionov, A. G. 1967. On the Connection between the Condensation Activity of Irradiated Nuclei and their Sizes. Atmos. Ocean. Phys. 3:25-33.

Laktionov, A. G. 1972. A Constant-Temperature Method of Determining the Concentrations of Cloud Condensation Nuclei. Atmos. Ocean. Phys. 8:672-677.

Laktionov, A. G. 1973. Spectra of Cloud Condensation Nuclei in the Supersaturation Range 0.02-1%. Proc. VIII Intl. Conf. on Nucleation, Leningrad, USSR, 437-444.

Langsdorf, A. Jr. 1936. A Continuously Sensitive Cloud Chamber. Phys. Rev. 49:422.

McCartney, H. A. and M. H. Unsworth. 1977. Spectral Distribution of Solar Radiation I: Direct Radiation. Quart. J. Roy. Meteor. Soc. 104:699-718.

Marlow, W. H. 1980. Introduction: The Domain of Aerosol Physics. "Aerosol Microphysics I," W. H. Marlow, Ed., Springer-Verlag, 1-14.

Mason, B. J. 1954. Bursting of Air Bubbles at the Surface of Sea Water. Nature. 174:470-471.

Mason, B. J. 1960. Ice-Nucleating Properties of Clay Minerals and Stony Meteorites. Quart. J. Roy. Meteor. Soc. 86:552-556.

Pruppacher, H. R. and J. D. Klett. 1980. "Microphysics of Clouds." D. Reidel. 714 pp.

Radke, L. F., S. K. Domonkos and P. V. Hobbs. 1981. A Cloud Condensation Nucleus Spectrometer Designed for Airborne Measurements. Third Intl. Cloud Condensation Nuclei Workshop, Reno, Navada, 6-17 October 1980, NASA Conf. Pub. 2212.

Rahn, K. A. and R. J. McCaffrey. 1981. Long Range Transport of Pollution Aerosol to the Arctic: A Problem Without Borders. World Meteor. Organ., WMO-No. 538:25-35.

Robinson, N. F. and W. T. Scott. 1981. Two-Stream Maxwellian Kinetic Theory of Cloud Droplet Growth by Condensation. J. Atmos. Sci. 38:1015-1026.

Rogers, R. R. 1979. "A Short Course in Cloud Physics." Pergamon Press. 232 pp.

Ryznar, E., M. R. Weber and T. Hallaron. 1981. Effects of the Mount St. Helens Volcanic Cloud on Turbidity at Ann Arbor, Michigan. J. Appl. Meteor. 20:1290-1294.

Saxena, V. K. and J. L. Kassner, Jr. 1970. Thermal Diffusion Chambers as Cloud Nuclei Counters. AEC Symposium Series, June 1-5, 1970. 217-238.

Saxena, V. K. and J. C. Carstens. 1971. On the Operation of Cylindrical Thermal Diffusion Cloud Chambers. J. Rech. Atmos. 5:11-23.

Schaefer, V. J. 1952. Induced Precipitation and Experimental Meteorology. Trans. New York Acad. Sci. 12:260-264.

Schaefer, V. J. 1969. The Inadvertent Modification of the Atmosphere by Air Pollution. Bull. Amer. Meteor. Soc., 50:155-206.

Schaefer, V. 1971. Remarks. Second International Workshop on Condensation and Ice Nuclei., Ft. Collings, CO., 5-19 August 1970, Compiled by L. O. Grant, 6-7.

Schaefer, V. J. 1981. Welcoming Address. Third International Cloud Condensation Nuclei Workshop, Reno, Nevada 6-17 October, 1980. NASA Conf. Pub. 2212, Edited by Kochmond, W. C., Rogers, C. F. and Rea, S. W. 4-5.

Schlichting, H. 1968. "Boundary Layer Theory." McGraw-Hill 653 pp.

Sedunov, Yu. S. 1974. "Physics of Drop Formation in the Atmosphere." Halsted Press. 234 pp.

Severynse, G. T. 1964. A Portable Cloud Nuclei Counter. J. Rech. Atmos. 1:11-16.

Sinnarwalla, A. M. and D. J. Alofs. 1973. A Cloud Nucleus Counter with Long Available Growth Time. J. Appl. Meteor. 12:831-835.

Squires, P. 1952. The Growth of Cloud Drops by Condensation. Aust. J. Sci. Res. A5:59-86.

Squires, P. 1971. Keynote Address. Second International Workshop on Condensation and Ice Nuclei at Ft. Collins, CO., 5-19 August 1970, compiled by Grant, L. O. 7-10.

Twomey, S. 1959. The Nuclei of Natural Cloud Formation - Part II: The Supersaturation in Natural Clouds and the Variation of Cloud Droplet Concentration. Geofis. Pura Appl. 43:243-249.

Twomey, S. 1963. Measurements of Natural Cloud Nuclei. J. Rech. Atmos. 1:101-105.

Twomey, S. A. 1981. Welcoming and Keynote Address. Third International Cloud Condensation Nuclei Workshop, at Reno, Nevada, 6-17 October, 1980. NASA Conf. Pub. 2212, edited by Kochmond, W. C. Rogers, C. F., and Rea, S.W. 4-5.

Vietti, M. A. and B. G. Schuster. 1973. Laser Scattering Measurement of Droplet Growth in Binary Mixtures. I. H_2O and Air. J. Chem. Phys. 58:434-441.

Wallace, J. M. and P. V. Hobbs. 1977. "Atmospheric Science." Academic Press. 467 pp.

Wieland, W. 1956. Condensation of Water Vapor on Natural Aerosol at Slight Supersaturation. Z. Angew. Math. Phys. 7:428-460.

APPENDIX

8. NUMERICAL MODEL TO DETERMINE VELOCITY PROFILE

This numerical model computes the steady state velocity in MOBIFOC with moving sidewalls. The coordinate system and boundary conditions used are shown in Figure 8.1. The equations used are taken from Bird et al. (1964) and are shown below:

$$\text{Equation of Motion:} \quad \rho\frac{dU}{dt} = -\nabla P + \mu\nabla^2 U + \rho g \tag{8.1}$$

$$\text{Equation of Continuity:} \quad \frac{\partial \rho}{\partial t} + \nabla\cdot(\rho U) = 0 \tag{8.2}$$

where:

ρ = density of air

P = pressure

μ = viscosity of air

g = gravitational acceleration

U = velocity of air = $u\hat{i} + v\hat{j} + w\hat{k}$

Under steady state, the boundary conditions are:

1. $0 \leq x \leq a$
2. $0 \leq y \leq b$
3. $0 \leq z \leq c$
4. $U(0,y,z) = V$
5. $U(a,y,z) = V$
6. $U(x,0,z) = 0$
7. $U(x,b,z) = 0$
8. $P(z=c) < P(z=0)$

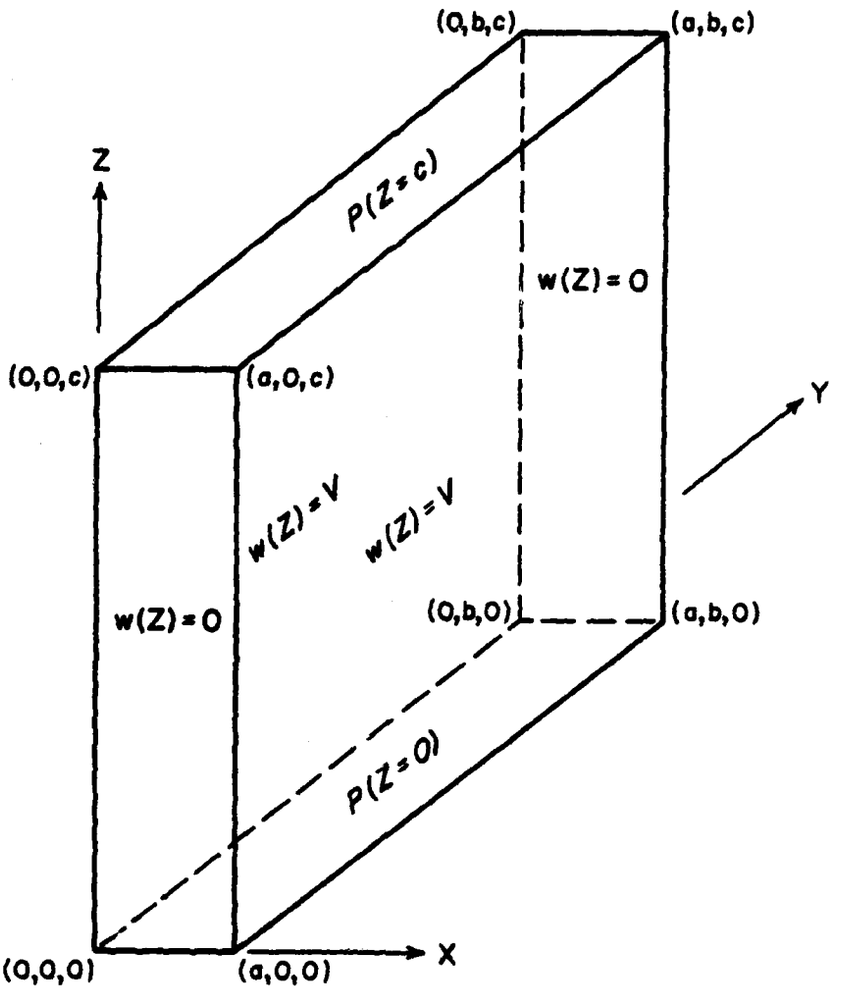

Figure 8.1 Boundary conditions for determination of velocity profiles.

Furthermore, if we assume that laminar flow exists, velocity in the vertical is constant ($\frac{\partial U}{\partial z} = 0$) and that ρ, μ, and g are constant then mass is conserved and (8.2) vanishes. (8.1) may now be expanded and incorporating the assumptions and boundary conditions we have

$$\frac{\partial^2 w}{\partial x^2} + \frac{\partial^2 w}{\partial y^2} = \frac{1}{\mu}\frac{\partial P}{\partial z} - \frac{\rho g}{\mu} . \tag{8.3}$$

Under the steady state conditions, $P(z=c)-P(z=0) = \frac{\partial P}{\partial z}$ = constant and therefore, the right hand side of (8.3) may be written as:

$$\frac{1}{\mu}\frac{\partial P}{\partial z} - \frac{\rho g}{\mu} = k \tag{8.4}$$

Substituting (8.4) into (8.3) we now have

$$\frac{\partial^2 w}{\partial x^2} + \frac{\partial^2 w}{\partial y^2} = k \tag{8.5}$$

which is the equation we must solve to determine the steady state velocity profiles.

In order to solve (8.5) we must first determine a value for the constant, k. We know (Schlicting, 1968) that the velocity between two infinitely long parallel plates is the sum of the induced flow of one plate in motion and forced flow due to an applied pressure differential. We therefore assume that this additive property holds within our chamber. In the case of plug flow, the velocity across the center of the chamber between the moving belts (i.e., at y=b/2) is uniform and therefore $\frac{\partial^2 w}{\partial y^2} = 0$. Substituting this into (8.5) we get:

$$\frac{\partial^2 w}{\partial x^2} = k \tag{8.6}$$

Integrating both sides twice, we get

$$w(x) = \frac{kx^2}{2} + \alpha x + \nu \tag{8.7}$$

In order to satisfy the boundary conditions, which in this case are w(0)=V and w(a)=V we find that

$$\nu = V$$

and

$$\alpha = -ka/2$$

and therefore

$$w(x) = \frac{kx^2}{2} - \frac{kax}{2} + V \tag{8.8}$$

or

$$k = \frac{2[w(x) - v]}{x^2 - ax} \tag{8.9}$$

Therefore, to find the value of k, we substitute the desired velocity at the center of the chamber (at x=a/2) for w(x) and the desired value for V into (8.9). Clearly at w(x)=V in (8.9), k=0. Using this value of k in (8.4) yields hydrostatic balance, or in other words, no vertical flow. Therefore, pure plug flow is not possible. However, we can settle for a nearly plug flow simply by making the velocity slightly higher than that of the belts. We therefore arbitrarily choose a value for w(x) at x=a/2 such as w(a/2)=1.001V where V is in cms^{-1}.

With this value of k, we can now establish the boundary conditions as:

1. $w(o,y) = V$
2. $w(a,y) = V$
3. $w(x,0) = 0$
4. $w(x,b) = 0$
5. $a = 2$ cm
6. $b = 20$ cm
7. $k = -.002\ cm^{-1}s^{-1}$

We may now solve (8.5) by the numerical method of relaxation. The SOR (simultaneous over-relaxation) method was used. The North Carolina State University Computer was used to generate solutions since the CAIL's TRS-80 was inadequate for this application.

Several solutions for $w(x,y)$ were generated for various values of V and k. Regardless of the value of V, the same velocity profile results for the same value of k. As k is decreased (i.e., forced flow becomes greater) a larger deviation from plug flow is evident. The solution shown in Chapter 3 (Figures 3.4 and 3.5) is based on $k = -.002cm^{-1}s^{-1}$.